

# Bcl-x<sub>L</sub> mediates RIPK3-dependent necrosis in *M. tuberculosis*-infected macrophages

X Zhao<sup>1,4</sup>, N Khan<sup>2,4</sup>, H Gan<sup>1</sup>, F Tzelepis<sup>2</sup>, T Nishimura<sup>1,3</sup>, S-Y Park<sup>1</sup>, M Divangahi<sup>2</sup> and HG Remold<sup>1</sup>

Virulent *Mycobacterium tuberculosis* (*Mtb*) triggers necrosis in host M $\phi$ , which is essential for successful pathogenesis in tuberculosis. Here we demonstrate that necrosis of *Mtb*-infected M $\phi$  is dependent on the action of the cytosolic Receptor Interacting Protein Kinase 3 (RIPK3) and the mitochondrial Bcl-2 family member protein B-cell lymphoma—extra large (Bcl-x<sub>L</sub>). RIPK3-deficient M $\phi$  are able to better control bacterial growth *in vitro* and *in vivo*. Mechanistically, cytosolic RIPK3 translocates to the mitochondria where it promotes necrosis and blocks caspase 8-activation and apoptosis via Bcl-x<sub>L</sub>. Furthermore, necrosis is associated with stabilization of hexokinase II on the mitochondria as well as cyclophilin D-dependent mitochondrial permeability transition. Collectively, these events upregulate the level of reactive oxygen species to induce necrosis. Thus, in *Mtb*-infected M $\phi$ , mitochondria are an essential platform for induction of necrosis by activating RIPK3 function and preventing caspase 8-activation.

## INTRODUCTION

Cell death is triggered by regulated and highly specific intracellular and extracellular signals. Apoptosis and necrosis are two major forms of cell death that have a critical role in immunity to infection by *Mycobacterium tuberculosis* (*Mtb*).<sup>1</sup> These distinct cell death modalities of macrophages (M $\phi$ ) directly affect control of *Mtb* growth and dissemination<sup>2–4</sup> as well as antigen-specific T-cell-mediated immunity via cross-presentation.<sup>5–8</sup> Thus it is not surprising that virulent strains of *Mtb* have developed mechanisms that allow evasion of M $\phi$  apoptosis by inducing necrosis.<sup>1</sup> Furthermore, we and others have demonstrated that during infection with *Mtb*, mitochondrial function is critical in determining the cell death modality.<sup>2,9–11</sup> Infection of human M $\phi$  with the attenuated *Mtb* H37Ra predominantly induces apoptosis,<sup>2,3,12</sup> which is dependent on mitochondrial outer membrane permeabilization and release of mitochondrial cytochrome c into the cytosol.<sup>11</sup> In contrast, infection of M $\phi$  with the virulent *Mtb* strain H37Rv induces necrosis<sup>2,3</sup> associated with irreversible permeabilization of the mitochondrial inner membrane leading to mitochondrial permeability transition (MPT) and loss of

mitochondrial integrity as well as function.<sup>11</sup> The MPT is regulated by calcium and occurs after opening of a functional pore, that includes the adenine nucleotide translocator (ANT), and a voltage-dependent anion channel (VDAC), whose functions are regulated by cyclophilin D (CypD).<sup>13,14</sup> CypD is a member of the cyclophilin family of peptidyl-prolyl *cis-trans* isomerases and has been implicated in MPT-dependent necrotic (but not apoptotic) cell death.<sup>15,16</sup> We have previously shown that CypD is involved in induction of *Mtb*-dependent M $\phi$  necrosis, which allows bacterial growth in virulent *Mtb*-infected cells.<sup>10</sup> These studies collectively indicate that programmed necrosis is essential for evasion of immunity by *Mtb* and is regulated at the level of mitochondria but the molecular mechanisms involved in the necrotic pathway remain elusive.

It has recently been shown that inhibitors of apoptosis (e.g., IAP) trigger formation of a complex including RIPK3 and RIPK1, which induces a type of necrosis referred to as necroptosis.<sup>17</sup> RIPK3-dependent necrosis seems to be tightly regulated by caspase 8<sup>18</sup> as it was shown that caspase 8 inactivates RIPK3.<sup>19</sup> Interestingly, an elegant study in a murine

<sup>1</sup>Division of Rheumatology, Immunology and Allergy, Department of Medicine, Brigham and Women's Hospital, Harvard Medical School, Boston, Massachusetts, USA.

<sup>2</sup>Department of Medicine, Department of Microbiology and Immunology, McGill International TB Centre, McGill University Health Centre, Meakins-Christie Laboratories, Montreal, Quebec, Canada and <sup>3</sup>Health Center, Keio University, Tokyo, Japan. Correspondence: HG Remold (hremold@partners.org) or M Divangahi (maziar.divangahi@mcgill.ca)

<sup>4</sup>These authors equally contributed to this work.

Received 5 May 2016; accepted 13 January 2017; published online 12 April 2017. doi:10.1038/mi.2017.12

tumor model recently has demonstrated that RIPK3-mediated necroptosis is more efficient in cross-priming CD8<sup>+</sup> T cells than apoptosis and within those dying cells RIPK1 signaling is required for initiating T-cell-mediated immunity.<sup>20</sup> Death-associated molecular patterns released from necroptotic cells also provoke a strong inflammatory response.<sup>21</sup> However, little is known about the role of the RIPK3 mediated cell death program during host interaction with a living pathogen that initiates multiple complex signaling pathways.

NAD(P)H oxidases (NOX) family of enzymes and mitochondria are the major intracellular sources of ROS.<sup>22</sup> ROS is produced in the mitochondria predominantly by the complexes I–III of the electron transport chain and by mitochondrial dehydrogenases including glycerol-3-phosphate dehydrogenase and  $\alpha$ -ketoglutarate dehydrogenase, a Krebs cycle enzyme,<sup>23</sup> which produces NADH and generates ROS if the NADH/NAD<sup>+</sup> ratio is high.<sup>24</sup> Processing of glucose is initiated by enzymes of the hexokinase (HK) family, which has four isoforms (HK-I to HK-IV). HK-II is critical for mitochondrial energy production since its presence on the outer mitochondrial membrane couples glycolysis with oxidative phosphorylation.<sup>25</sup> Augmented levels of HK-II increase ROS accumulation if the normal function of the mitochondrial electron chain is compromised. Interestingly, increased mitochondrial ROS production has been associated with RIPK3-dependent necrosis.<sup>26</sup> Moreover, the mitochondrial Bcl-2 family protein B-cell lymphoma-extra large (Bcl-x<sub>L</sub>) on the mitochondria is known to block apoptosis by inhibiting the function of Bcl-2 homologous antagonist/killer (BAK)<sup>27</sup> via blocking Bcl-2-associated X protein (BAX) recruitment to the mitochondria.<sup>28,29</sup>

Here we report that in M $\phi$  infected with virulent *Mtb*, RIPK3 translocates to mitochondria as evidenced by its presence in mitochondria along with Bcl-x<sub>L</sub> and pro-caspase 8. Mitochondrial pro-caspase 8 in the presence of RIPK3 and Bcl-x<sub>L</sub> remains in its inactive zymogen form, suggesting that Bcl-x<sub>L</sub> is critical for preventing caspase 8-mediated apoptosis and that the presence of active RIPK3 on the mitochondria is required for induction of necrosis. Furthermore, we identify RIPK3 as a kinase involved in the induction of necrosis impairing host M $\phi$  immunity both *in vitro* and *in vivo*. Interestingly, the enhanced protection of RIPK3-deficient mice was independent of T-cell-mediated immunity to pulmonary *Mtb* infection. Collectively, our findings demonstrate that following *Mtb* infection RIPK3 is involved in the activation of several independent mechanisms that ultimately converge at the inhibition of apoptosis and promotion of necrosis in M $\phi$ , which enhances the susceptibility of the host to infection.

## RESULTS

### RIPK3 is required for induction of necrosis in M $\phi$ infected with virulent *Mtb*

A hallmark of M $\phi$  infection with virulent *Mtb* is necrosis, which allows the bacteria to evade the host defense mechanisms.<sup>1</sup> RIPK3 is required for the induction of necrosis in a variety of cell models.<sup>18</sup> To test whether a RIPK3-dependent pathway is

directly involved in necrosis and innate control of virulent H37Rv infection, we silenced the *RIPK3* gene in human M $\phi$  using two different RIPK3 siRNAs (**Figure 1a** and **Supplementary Figure 1A** online). In the absence of RIPK3, necrosis was remarkably reduced in *Mtb*-infected M $\phi$  (**Figure 1b** and **Supplementary Figure 1A**). This reduction of necrotic cell death also correlated with decreased bacterial growth in RIPK3-deficient M $\phi$  (**Figure 1c**). Because of potential off-target effects of siRNA, we performed similar experiments using RIPK3-deficient mice. Similar to human M $\phi$ , *Mtb*-infected RIPK3-deficient murine M $\phi$  revealed decreased necrosis (**Figure 1d**), which led to significant reduction of bacterial growth *in vitro* (**Figure 1e**). Decreased necrosis in RIPK3<sup>-/-</sup> M $\phi$  was also associated with significant reduction of extracellular bacteria compared with *Mtb*-infected wild-type (WT) M $\phi$  (**Figure 1f**). To determine whether reduced necrosis also occurs in the lungs of RIPK3<sup>-/-</sup> mice following *Mtb* infection, we infected RIPK3<sup>-/-</sup> and WT mice via the intratracheal route with H37Rv and collected bronchoalveolar lavage 2 days after infection. The levels of dead cells were significantly lower in the lungs of infected RIPK3<sup>-/-</sup> mice than WT mice (**Figure 1g**). We next investigated the involvement of the mixed lineage kinase domain-like protein (MLKL), which is a substrate for RIPK3 kinase activity to mediate necrosis.<sup>30</sup> Interestingly, the levels of MLKL were increased in human M $\phi$  infected with H37Rv (**Figure 1h**) and silencing of MLKL significantly decreased necrosis in H37Rv-infected M $\phi$  (**Figure 1i** and **Supplementary Figure 1B**). Collectively, these data from both *in vitro* human and murine M $\phi$  as well as the *in vivo* experiments indicate that RIPK3 plays a critical role in the necrosis pathway during the course of *Mtb* infection.

### RIPK3 and pro-caspase 8 translocate from the cytosol to the mitochondria in *Mtb*-infected M $\phi$

In cells undergoing genotoxic stress pro-caspase 8 forms a cytosolic complex with RIPK1, RIPK3 and FADD termed the “ripiptosome”, which can become a cytosolic cell death signaling platform.<sup>17,31</sup> We therefore investigated whether a similar complex exists in human M $\phi$  infected with *Mtb*. Here we found that RIPK1, RIPK3, and pro-caspase 8 co-precipitate in the cytosol but not on mitochondria of human M $\phi$  prior to infection (**Figure 2a**, **Supplementary Figure 3A**) similar to the ripiptosome. At 2 h after infection of human M $\phi$  with virulent H37Rv or avirulent H37Ra, we observed that RIPK3, RIPK1 and pro-caspase 8 translocate from the cytosol to the mitochondria (**Figure 2a**, right lane). In H37Rv-infected pro-necrotic M $\phi$ , the levels of pro-caspase 8 and RIPK3 increased on the mitochondria over time (**Figure 2b**). In contrast, in M $\phi$  infected with the avirulent H37Ra, the levels of pro-caspase 8 and RIPK3 on the mitochondria were markedly reduced by 24 h, which is consistent with pro-caspase 8 becoming activated at 24 h to induce apoptosis (**Figure 2c**). The translocation of cytosolic RIPK3 and pro-caspase 8 to the mitochondria cannot be explained by contamination of the mitochondrial fractions with

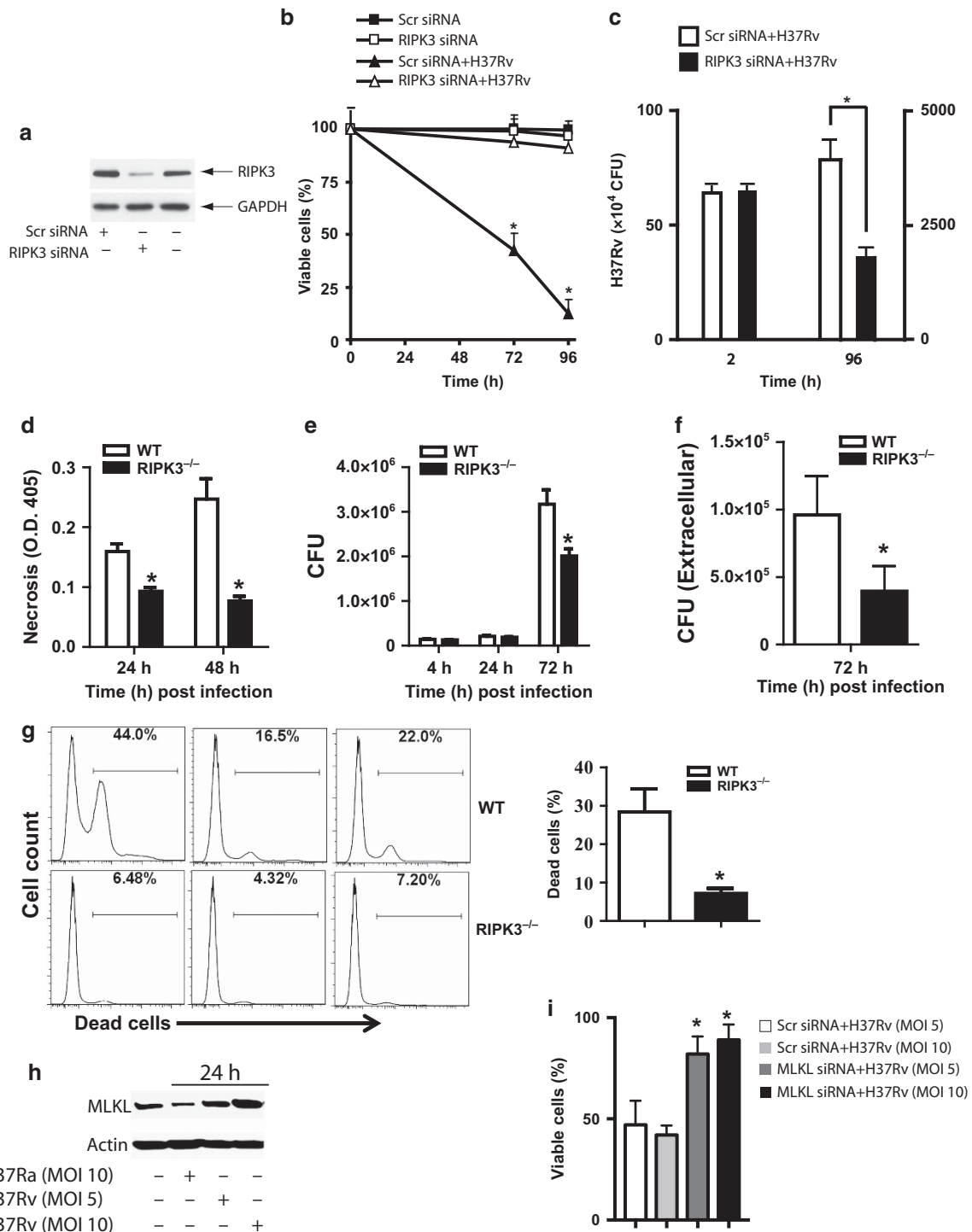


**Figure 1** RIPK3 impairs anti-mycobacterial defense mechanisms in *Mtb*-infected M $\phi$ . (a) Silencing efficiency of RIPK3 siRNA. Aliquots (50  $\mu$ g) of cell lysates from human M $\phi$  treated with targeted RIPK3 siRNA or with control scrambled siRNA (Scr) were collected 12 h post-transfection and subjected to western blot analysis of RIPK3 levels. GAPDH was used as a loading control. (b) Human M $\phi$  transfected with scrambled control (Scr) or RIPK3 siRNA (RIPK3 siRNA) were infected with H37Rv (MOI 5) and the cell viability was evaluated at 0 to 96 h after infection. (c) Human M $\phi$  treated with scrambled (Scr) or RIPK3 siRNA were infected with H37Rv (MOI 5) and the replication of H37Rv was measured at 2 and 96 h post infection. (d) BMD-M $\phi$  from WT and RIPK3<sup>-/-</sup> mice were infected with H37Rv at an MOI of  $\sim$ 5. After 24 and 48 h, necrosis was assessed using a commercially available Cell Death ELISA kit (Roche). (e and f) After 72 h, the growth of intracellular bacteria (e) and the number of extracellular bacteria (f) was significantly reduced in RIPK3<sup>-/-</sup> M $\phi$ . (g) WT and RIPK3<sup>-/-</sup> mice ( $n=3$  per group) were intratracheally infected with H37Rv ( $0.5 \times 10^5$  CFU) and then BAL was performed after 48 h of infection. Cell death was assessed using Live/Dead fixable dead cell stain kits (Invitrogen). Each histogram is representative of the BAL from an individual infected mouse and the numbers in histograms indicate the percentage of dead cells. (h) Increased expression of MLKL in H37Rv infected human M $\phi$ . (i) Human M $\phi$  treated with MLKL siRNA or scrambled RNA (scr) were infected with H37Rv (MOI 5 or 10) and the cell viability was evaluated at 72 h after infection. Results are expressed as mean  $\pm$  s.d. Data were analyzed using one-way ANOVA. \*, Values of  $P < 0.05$  were considered to be significant. Data are representative of 2–3 independent experiments. ANOVA, analysis of variance; BAL, bronchoalveolar lavage.

cytosolic proteins, because mitochondrial preparations from uninfected M $\phi$  did not contain significant amounts of RIPK1, RIPK3 and pro-caspase 8 (**Figure 2a**). Moreover, using fluorescence confocal microscopy we demonstrated that the levels of pro-caspase 8 and RIPK3 colocalization were significantly increased in M $\phi$  infected with the virulent H37Rv strain (**Figure 2d and e**). Additionally, the levels of cleaved caspase 8 was significantly higher in H37Rv-infected RIPK3-deficient M $\phi$  compared with WT M $\phi$  (**Figure 2f**) while there was no difference in M $\phi$  infected with H37Ra (**Supplementary Figure 2A**). These data indicate that after infection of M $\phi$  with virulent *Mtb* the mitochondria acquire a complex containing RIPK1, RIPK3 and pro-caspase 8 where RIPK3 was required to prevent caspase 8 activation.

### RIPK3 and Bcl-x<sub>L</sub> prevent activation of pro-caspase 8 on the mitochondria promoting necrosis in *Mtb*-infected M $\phi$

Bcl-x<sub>L</sub> protects mitochondria against apoptosis by inhibiting BAK activation.<sup>28</sup> RIPK3 and pro-caspase 8 translocate to the mitochondria in H37Rv-infected M $\phi$  as shown by their presence in mitochondrial fractions after 6 and 24 h of infection (**Figure 3a**). Bcl-x<sub>L</sub> was required for the sequestration of pro-caspase 8 on the mitochondria in its inactive form, as silencing of the Bcl-x<sub>L</sub>-gene led to proteolytic processing of pro-caspase 8 and disappearance of RIPK3 from the mitochondria 24 h post-H37Rv-infection (**Figure 3a**). In contrast, 24 h after infection of M $\phi$  with avirulent H37Ra (which promotes apoptosis), the Bcl-x<sub>L</sub> levels on the mitochondria were significantly diminished, which was also associated with disappearance of pro-caspase 8 and RIPK3 from the mitochondria (**Figure 3b**). These findings are in agreement with a study demonstrating that by outcompeting Bax via Bcl-x<sub>L</sub>, cells are protected against apoptosis.<sup>28</sup> Finally, we demonstrated that silencing Bcl-x<sub>L</sub> in H37Rv-infected M $\phi$  significantly reduced necrosis (**Figure 3c** and **Supplementary Figure 1C**). These experiments collectively indicate that the presence of RIPK3 and Bcl-x<sub>L</sub> on the mitochondria is required to inhibit caspase 8 activation, which leads to increase necrosis in *Mtb*-infected M $\phi$ .

The dual function of caspase 8 in initiation of apoptosis and suppression of RIPK3-dependent necrosis,<sup>32–34</sup> which has been shown to be required for normal murine embryonic development and survival<sup>35</sup> is well documented. Active caspase 8 blocks necrosis by proteolytically inactivating RIPK1 and RIPK3.<sup>19,36,37</sup> Thus we next inhibited the apoptotic pathway in H37Ra-infected M $\phi$  using the caspase inhibitor z-IETD-FMK and then measured the levels of mitochondria-associated RIPK3. As expected, in M $\phi$  infected with avirulent H37Ra, pro-caspase 8 (**Figure 3b**) and both apoptosis-executor caspases 9 and 3 were not activated in the presence of z-IETD-FMK (**Figure 3d**) confirming an essential role for the caspases 8, 9 and 3 in apoptosis of *Mtb*-infected M $\phi$ . Importantly, in H37Ra-infected M $\phi$  treated with z-IETD-FMK the levels of mitochondria-associated RIPK3, Bcl-x<sub>L</sub>, and pro-caspase 8 were all increased to the similar levels found in M $\phi$  infected with the virulent strain H37Rv (**Figure 3b**)

indicating that inhibition of caspase 8, 9 and 3-activation is required for the RIPK3-dependent necrotic pathway to be initiated.

Finally, to test whether RIPK3 is also required for regulation of Bcl-x<sub>L</sub>-mediated pro-caspase 8-persistence on the mitochondria, we next silenced the *RIPK3* gene in H37Rv-infected M $\phi$ . At 24 h after infection, reduction of mitochondrial Bcl-x<sub>L</sub>-accumulation correlated with reduced pro-caspase 8-accumulation on the mitochondria (**Figure 3e**) suggesting that proteolytic processing of pro-caspase 8 initiates apoptosis. In addition, silencing *RIPK3* leads to caspase 3-activation, which is a key indicator of apoptosis (**Figure 3f**). In contrast to H37Rv infection, apoptosis was significantly increased in H37Ra-infected M $\phi$  as measured by caspase 8 and 3 activation (**Supplementary Figure 2A–C**) as well as increased apoptotic surface markers (**Supplementary Figure 2D**). Thus the presence or absence of RIPK3 had no significant effect on the apoptosis of M $\phi$  infected with H37Ra. Collectively these data indicate that induction of necrosis in *Mtb*-infected M $\phi$  is critically dependent on blocking activation of pro-caspases 8-, 9- and 3-mediated apoptosis via RIPK3.

To determine whether caspase 8-activation is part of the intrinsic mitochondria-dependent apoptotic pathway, which includes activation of BID to tBID and depends on BAX,<sup>29</sup> we next evaluated activation of BID and BAX in M $\phi$  infected with H37Ra or H37Rv. After 10 min of infection with H37Ra, pro-caspase 8-activation led to formation of tBID on the mitochondria (**Figure 3g**, right). However, tBID was not detectable on the mitochondria of H37Rv-infected M $\phi$  (**Figure 3g**, left). Most importantly, silencing of the *BAX* gene in H37Ra-infected M $\phi$  inhibited apoptosis-executor caspase 3 activation (**Figure 3h**). This indicates that activation of pro-caspase 8 on the mitochondria is initiated by the intrinsic apoptotic pathway via BAX translocation, which is part of the mitochondrial amplification loop of apoptosis and triggers degradation of RIPK3 from the mitochondria.

### RIPK3 mediates hexokinase II translocation to the mitochondria via Bcl-x<sub>L</sub> in H37Rv-infected M $\phi$

As RIPK3 regulates ROS production following TNF- $\alpha$  treatment and because ROS have an important role in regulation of cell death programs,<sup>26</sup> we next studied whether necrosis in *Mtb*-infected M $\phi$  is ROS-dependent. We found that ROS accumulation in M $\phi$  infected with virulent H37Rv was significantly increased in comparison with M $\phi$  infected with the avirulent strain H37Ra (**Figure 4a**). RIPK3 was required to increase ROS accumulation in H37Rv-infected M $\phi$  because silencing of the *RIPK3* gene significantly reduced ROS production (**Figure 4b**). This increased production of ROS was independent of mitochondrial mass (data not shown). Increased ROS accumulation triggers necrosis in H37Rv-infected M $\phi$  because scavenging of ROS with Tiron significantly reduced necrosis (**Figure 4c**). As hexokinase II (HKII) binds to the VDAC in the mitochondrial outer membrane and is the limiting enzyme of glucose metabolism,<sup>25</sup> we next determined whether HKII contributes to ROS accumulation.



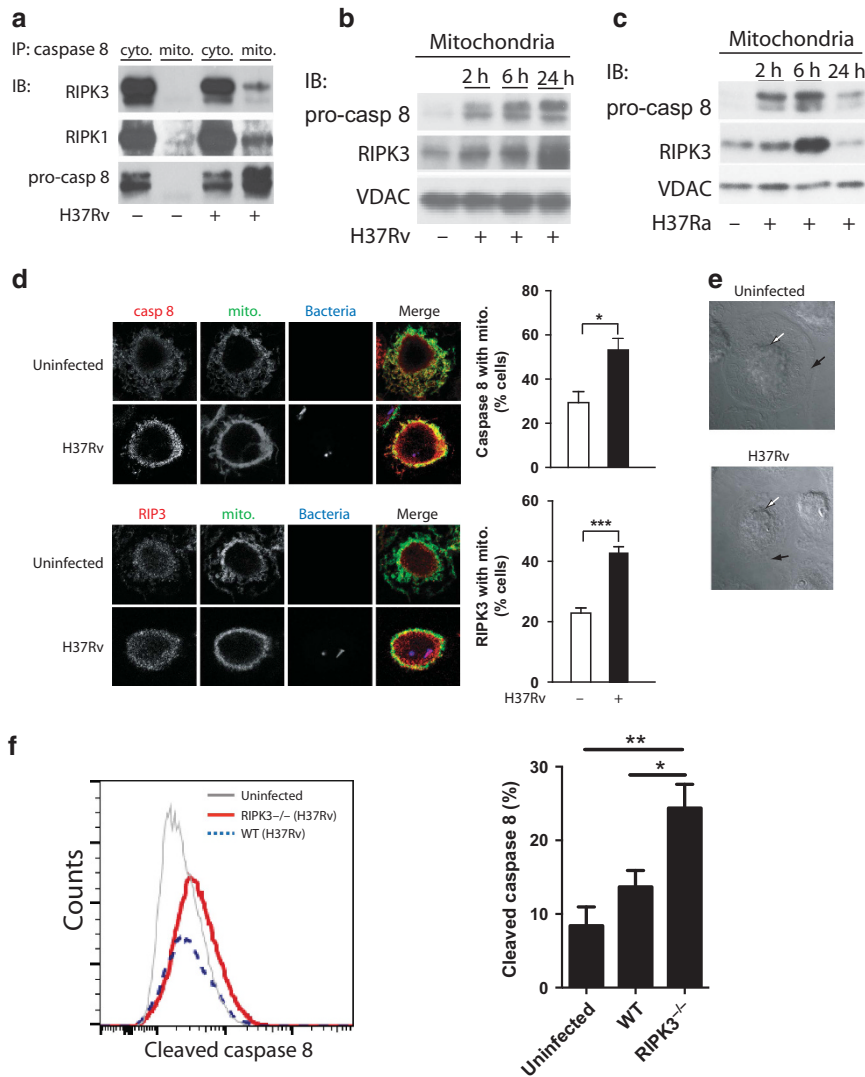


**Figure 2** Translocation of a RIPK3/pro-caspase 8 containing complex to the mitochondria of H37Rv-infected M $\phi$ . **(a)** Cytosolic and mitochondrial RIPK1, RIPK3 and pro-caspase-8 following H37Rv infection. Equal numbers of human M $\phi$  were infected with H37Rv (MOI 10) and lysed for isolation of cytosolic and mitochondrial fractions after 24 h of infection. Equal amounts of protein were immunoprecipitated (IP) with anti-caspase-8 ab and the levels of RIPK3, RIPK1, and pro-caspase 8 were measured by western blot analysis. **(b and c)** Time-dependent translocation of RIPK3 and pro-caspase 8 to the mitochondria. Equal numbers of M $\phi$  were infected with virulent H37Rv **(b)** or avirulent H37Ra **(c)** at MOI 10. The levels of pro-caspase 8 and RIPK3 were determined by subjecting equal amounts of mitochondria isolated from infected M $\phi$  to western blotting. VDAC was used as a loading control. **(d)** Colocalization of caspase 8 and RIPK3 with the mitochondria of H37Rv-infected M $\phi$ . **(left)** Colocalization of caspase 8 and pro-caspase 8 with mitochondria 24 h after infection visualized by confocal fluorescence microscopy. Human M $\phi$  remained either uninfected or were infected with mCherry-H37Rv (MOI 10) for 24 h, fixed and stained with mitotracker (green) and anti-RIPK3 or anti-caspase 8 ab (red). Scale bar, 30  $\mu$ m. On the right side of each panel is the quantification of caspase 8 **(top)** and of RIPK3 **(bottom)** associated with the mitochondria. Data were analyzed using nonparametric Student *t*-test **(e)** Phase-contrast images of representative infected and uninfected human primary M $\phi$  after 24 h of infection show approximate location of the plasma membrane and the nucleus as indicated by black and white arrows, respectively. Due to incipient necrosis the plasma membrane of the H37Rv-infected M $\phi$  is not clearly visible. **(f)** BMD-M $\phi$  from WT and RIPK3<sup>-/-</sup> mice were infected with H37Rv at an MOI of  $\sim$ 10. After 12 h, expression of cleaved caspase 8 was assessed using flowcytometry. Results are represented as mean  $\pm$  s.d. Data were analyzed using one-way ANOVA. \*, \*\*, \*\*\* Values of  $P < 0.05$ ,  $P < 0.01$ , and  $P < 0.001$ , respectively were considered to be significant. Data are representative of 2–3 independent experiments. ANOVA, analysis of variance.

Kinetic studies of HKII-translocation to the mitochondria indicated that the levels of HKII were significantly increased and maintained on the mitochondria of H37Rv-infected M $\phi$  compared with H37Ra-infected M $\phi$  **(Figure 4d)**. Increased binding of HKII to mitochondria in M $\phi$  infected with virulent H37Rv correlated with enhanced ROS production, which was reduced after *HKII* gene silencing **(Figure 4e)**. As NADH accumulation is required for ROS production in a HKII-

dependent manner,<sup>25</sup> NADH levels were subsequently diminished after silencing of the *HKII* gene and the *RIPK3* gene **(Supplementary Figure 3C and D)**. Further, NADH oxidase inhibitor Diphenyleneiodonium (DPI) abolished ROS production and reduced necrosis in H37Rv-infected M $\phi$  **(Figure 4f and g)**. Interestingly, in H37Rv-infected M $\phi$ , silencing of the *Bcl-x<sub>L</sub>* gene diminished HKII recruitment to the mitochondria at 24 h post infection **(Figure 4h)**, while silencing

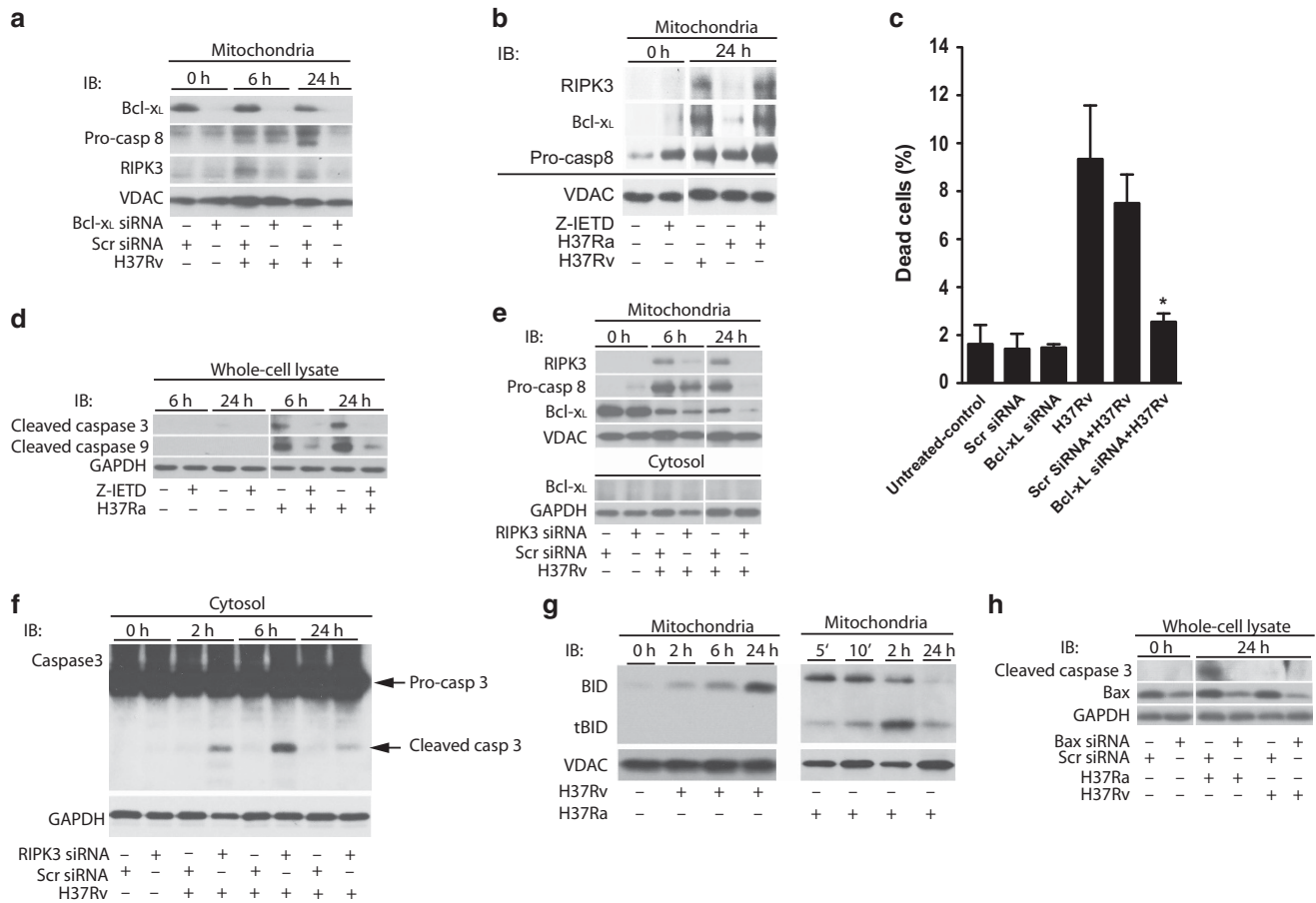


**Figure 3** Bcl-x<sub>L</sub> enables pro-caspase 8 and RIPK3 accumulation on mitochondria of *Mtb*-infected M $\phi$ . (a) Bcl-x<sub>L</sub> is required for pro-caspase 8 and RIPK3 accumulation on the mitochondria of H37Rv infected M $\phi$ . Human M $\phi$  were transfected with Bcl-x<sub>L</sub> or scrambled control (Scr) siRNA and then infected with H37Rv (MOI 10). Equal amounts of purified mitochondria from non-infected and H37Rv-infected M $\phi$  were subjected to Western blot analysis to determine the levels of pro-caspase 8 and RIPK3. (b) Caspase inhibition of H37Ra infected M $\phi$  enables RIPK3/Bcl-x<sub>L</sub> accumulation on mitochondria. After treatment with the caspase inhibitor z-IETD pro-caspase 8, RIPK3 and Bcl-x<sub>L</sub> accumulates on the mitochondria of H37Ra infected M $\phi$ . Mitochondria were isolated from H37Rv or H37Ra-infected M $\phi$  treated with or without z-IETD (10  $\mu$ M) and subjected to western blot analysis using anti caspase 8, anti-RIPK3 and anti-Bcl-x<sub>L</sub> antibodies. Equal amounts of the proteins were subjected to Western blot analysis for the evaluation of RIPK3 and Bcl-x<sub>L</sub> levels. (c) M $\phi$  treated with Bcl-x<sub>L</sub> or scrambled control siRNA (Scr) were infected with H37Rv (MOI 10) and cell death was assessed after 48 h using Live/Dead fixable dead cell stain kits (Invitrogen). (d) z-IETD blocks activation of the apoptotic caspases 9 and 3 essential for apoptosis induction. Equal amounts of cell lysates of M $\phi$  infected with H37Ra (pro-apoptotic strain) treated with or without z-IETD (10  $\mu$ M) were subjected to western blot analysis for evaluating active caspase 3 and 9. (e) RIPK3 is required for accumulation of mitochondrial pro-caspase 8 and Bcl-x<sub>L</sub>. Mitochondria and cytosolic fraction of H37Rv-infected M $\phi$  treated with RIPK3 or Scr siRNA were subjected to western blot analysis and the levels of RIPK3, pro-caspase 8 and Bcl-x<sub>L</sub> were evaluated. (f) Silencing of the RIPK3 gene activates apoptosis executor caspase 3 in H37Rv infected M $\phi$ . M $\phi$  treated with RIPK3 or Scr siRNA were infected with H37Rv. Cell lysate was collected and equal amounts subjected to Western blot analysis for cleaved caspase 3. (g) Bid processing in H37Ra and H37Rv-infected M $\phi$ . Mitochondria were isolated from H37Ra (right panel) or H37Rv (left) -infected M $\phi$  and the kinetics of BID processing and tBID accumulation were assessed by western blotting. (h) Silencing of the *BAX* gene in H37Ra-infected M $\phi$  blocks caspase 3 activation, a marker for apoptosis. M $\phi$  treated with BAX or Scr siRNA were infected with H37Ra or H37Rv (MOI 10). Cell lysate was collected after 0 and 24 h and equal amounts subjected to Western blot analysis for pro-caspase 3 and cleaved caspase 3. VDAC and GAPDH were used as a loading control. Results are expressed as mean  $\pm$  s.d. Data were analyzed using one-way ANOVA. \*, Values of  $P < 0.05$  were considered to be significant. Data are representative of four independent experiments.

of the *RIPK3* gene prevented HKII recruitment to the mitochondria as early as 6 h post infection that persisted up to 24 h post infection (Figure 4i). Collectively, these data indicate that in M $\phi$  infected with virulent *Mtb*, HKII translocation to the mitochondria mediates via Bcl-x<sub>L</sub> and RIPK3 that leads to increased ROS production.

#### RIPK3 mediates MPT in M $\phi$ infected with H37Rv

Increased mitochondrial permeability transition (MPT), a sign of mitochondrial damage, induces pyridine nucleotide release

from the mitochondria,<sup>38</sup> which decreases mitochondrial respiration and cellular ATP-levels, which leading to necrotic cell death.<sup>39</sup> MPT increases electron leakage predominantly from mitochondrial complex I and III and enhances ROS production in the presence of sufficient NADH.<sup>39</sup> We have previously shown that virulent *Mtb* induced MPT-dependent necrosis and that cyclosporin A (CsA), a selective inhibitor of the peptidyl-prolyl *cis-trans* isomerase activity of CypD, blocks MPT mediated necrosis.<sup>10,11,40-41</sup> The critical role of CypD in necrosis was demonstrated in *Ppif* null mice, which lack the

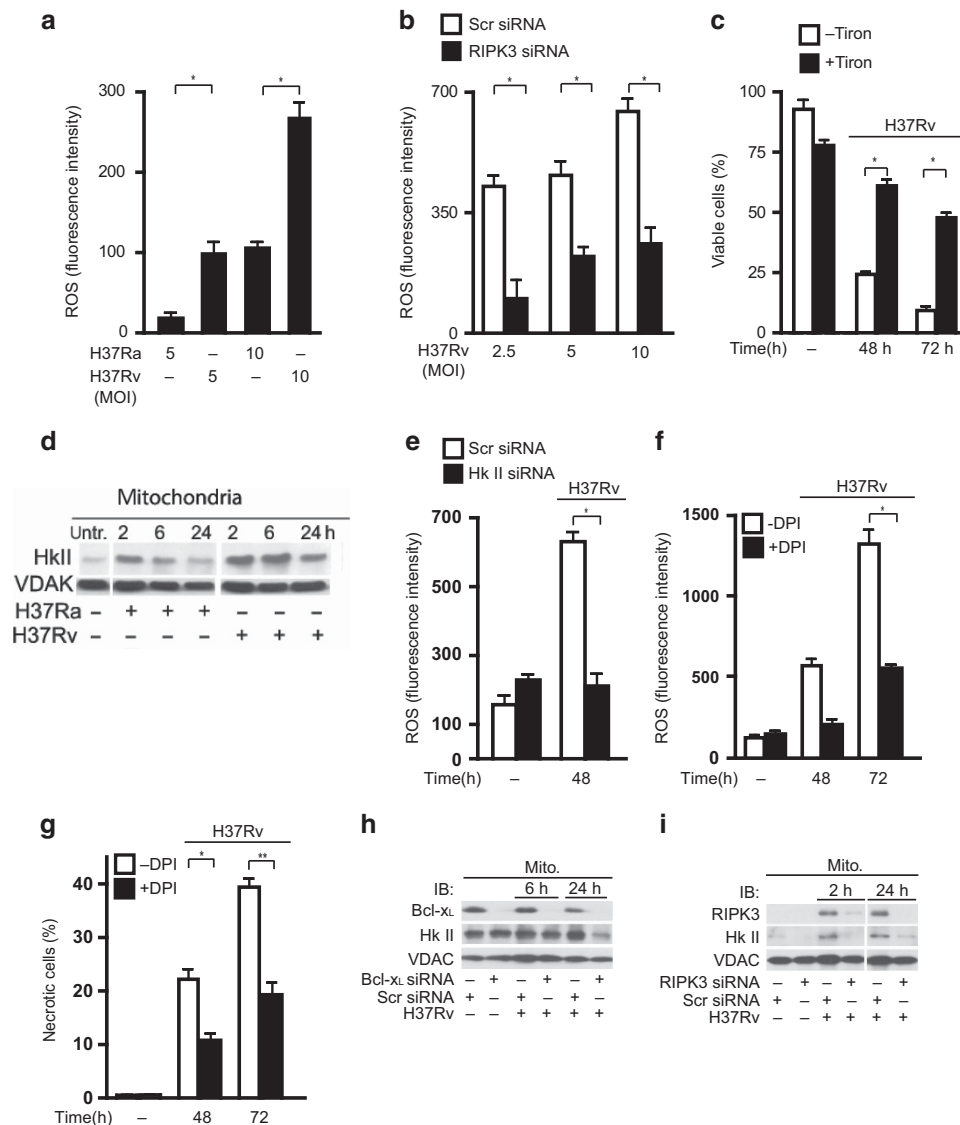


**Figure 4** RIPK3 is required for ROS-dependent necrosis in M $\phi$  infected with virulent *Mtb* via upregulation of mitochondrial HKII-levels. (a) M $\phi$  were infected with H37Ra or H37Rv (MOI 5 and 10) and after 48 h ROS accumulation was determined by FACS analysis using the fluorescent dye CM-H<sub>2</sub>XRos. (b) ROS production was significantly reduced in RIPK3 deficient M $\phi$  infected with H37Rv. Human M $\phi$  were transfected with RIPK3 or scrambled control siRNA infected with H37Rv (MOI 2.5, 5 and 10) and ROS accumulation was determined after 48 h of infection. (c) Scavenging ROS increases M $\phi$  viability following H37Rv infection. M $\phi$  were treated with or without 0.05 mM Tiron and infected with H37Rv (MOI 10). M $\phi$  viability was measured at 0, 48 and 72 h post-infection. Data are represented as mean  $\pm$  standard error. All experiments were repeated at least three times with similar results. (d) HKII recruitment to the mitochondria in H37Ra and H37Rv infected M $\phi$ . Equal amounts of mitochondrial extracts from H37Ra and H37Rv-infected M $\phi$  were subjected to western blot analysis of HKII at 0, 2, 6 and 24 h post-infection (top). (e) M $\phi$  were silenced with HKII siRNA or treated with scrambled control (Scr) siRNA and then infected with H37Rv (MOI 10:1). M $\phi$  deficient in HKII produced significantly less ROS after H37Rv infection. After 48 h ROS accumulation was determined by FACS analysis using the fluorescent dye CM-H<sub>2</sub>XRos. (f and g) M $\phi$  were treated with NADH oxidase inhibitor (DPI) for 2 h prior to infection with H37Rv (MOI 10) and ROS accumulation and viability was determined after 48 h and 72 h. (h) Silencing of the *Bcl-xL* gene in H37Rv-infected M $\phi$  prevents HKII recruitment to the mitochondria at 24 h after infection; (i) silencing of the *RIPK3* gene prevents HKII recruitment to the mitochondria at as early as 2 h post infection and at 24 h after infection. Mitochondria were isolated from H37Rv-infected M $\phi$  treated with RIPK3, or scrambled control siRNA and were then subjected to western blot analysis for HKII. MOI's for all experiments were 10:1. VDAC was used as a loading control. Results are expressed as mean  $\pm$  s.e. using the nonparametric Student *t*-test. \*, Values of  $P < 0.05$  were considered to be significant. Data are representative of three independent experiments. FACS, fluorescence-activated cell sorting.

gene encoding CypD, as these mice were protected against necrosis.<sup>15,16</sup> Thus we wondered whether there is a link between RIPK3, CypD, and MPT in *Mtb*-infected M $\phi$ . We first showed that silencing of the *RIPK3* gene blocked H37Rv-induced MPT in M $\phi$  after 48 and 72 h post infection (Figure 5a). Since we demonstrated that induction of MPT by RIPK3 was required

for initiation of necrosis, we next sought to determine how virulent *Mtb* initiates MPT. In H37Rv-infected M $\phi$  treatment with CsA inhibited ROS accumulation (Figure 5b) and necrosis (Figure 5c). We also found that in CsA-treated M $\phi$  infected with H37Rv, the levels of mitochondrial RIPK3, pro-caspase 8, Bcl-x<sub>L</sub>, and HKII were diminished (Figure 5d). However, in

H37Ra-infected M $\phi$  there was no interaction between mitochondrial CypD and ANT (**Figure 5e**). Moreover, immunoprecipitation of ANT from the mitochondria of H37Rv-infected M $\phi$  treated with CsA showed that CypD binding to ANT was completely abolished (**Figure 5f**). These data suggest that RIPK3 acts as a regulator of CypD function to induce MPT leading to inhibition of ATP generation and contributing to necrosis. To test whether RIPK3 causes MPT by initiating CypD-binding to ANT and MPT pore opening, we silenced *RIPK3* in H37Rv-infected M $\phi$  and assessed the interaction of CypD with ANT. In the absence of RIPK3 in H37Rv-infected M $\phi$  the CypD/ANT interaction was also diminished (**Figure 5g**), which correlated with the reduction of MPT (**Figure 5a**).

Thus RIPK3 induces necrosis in H37Rv-infected M $\phi$ , by at least two independent, but interrelated mechanisms: (1) RIPK3 increases Bcl-x<sub>L</sub>-dependent HKII recruitment to the mitochondria possibly leading to enhanced glucose consumption and increased NADH accumulation as well as ROS generation; and (2) RIPK3 induces MPT in a CypD-dependent manner, which in the presence of abundant NADH boosts accumulation of ROS by uncoupling of the mitochondrial electron chain.

#### RIPK3 deficient M $\phi$ mediate resistance to pulmonary *Mtb* infection

To translate our *in vitro* observation *in vivo*, we have utilized two models of *Mtb* infection. In the first model, mice were intravenously (IV) infected with a high dose of H37Rv ( $1 \times 10^6$  colony forming units (CFU)) and after 4 weeks of infection, we found a significant reduction in the pulmonary bacterial burden of RIPK3<sup>-/-</sup> compared to WT mice (**Figure 6a**). Interestingly, the number of neutrophils (cellular marker of necrotic lung tissues) was also significantly reduced in *Mtb*-infected RIPK3<sup>-/-</sup> mice (**Figure 6b, c** and **Supplementary Figure 4**). However, with the exception of TNF $\alpha$ , which was significantly reduced in RIPK3<sup>-/-</sup> mice, the expression levels of other cytokines, including IL-1 $\beta$ , IL-6, and IL-12 were not markedly changed (**Figure 6d**). In the second model, we aerosolized WT and RIPK3<sup>-/-</sup> mice with a low dose (~50 CFU) of the virulent strain H37Rv. Similar to IV-model, RIPK3<sup>-/-</sup> mice had significantly lower lung bacterial burden (~half log) after 5 weeks of infection (**Figure 7a**). Considering the important role of T cells in protection against *Mtb* infection, we next examined the potential contribution of T-cell-mediated immunity in protection of RIPK3<sup>-/-</sup> mice. Similar to other studies,<sup>20,42</sup> we also found that the presence or absence of RIPK3 had no effect on T cell proliferation *in vitro* (**Supplementary Figure 5A**). At 5 weeks post-*Mtb* infection there was no significant difference in frequency of pulmonary CD4<sup>+</sup>/CD8<sup>+</sup> T cells (**Figure 7b**) as well as TB10.4-specific CD8<sup>+</sup> T cells (**Figure 7c**) or ESAT6-specific CD4<sup>+</sup> T cells between WT and RIPK3<sup>-/-</sup> mice (**Figure 7d**). Moreover, there was no difference in total cell numbers of T cells or antigen-specific T cells (**Supplementary Figure 5B and C**). Furthermore, ELISPOT experiments revealed that the function of T cells was intact as they produced similar levels of IFN- $\gamma$

following stimulation with *Mtb*-antigens recognized by either CD4<sup>+</sup> or CD8<sup>+</sup> T cells (**Supplementary Figure 5D**). Thus these data indicate that the quantity and quality of T cells was not affected by RIPK3 and the increased protection of RIPK3<sup>-/-</sup> mice after *Mtb* infection was independent of T-cell-mediated immunity.

To directly evaluate the protective role of RIPK3 in M $\phi$  innate immunity in the absence of any contribution from adaptive immune responses, we utilized our established adoptive transfer model of *Mtb*-infected M $\phi$ .<sup>3,5,43</sup> We infected WT and RIPK3<sup>-/-</sup> murine alveolar M $\phi$  *in vitro* with a low dose of the virulent strain H37Rv (MOI ~ 1), then transferred the cells by the intratracheal route into recipient mice deficient in recombinase-activating gene 1 (*Rag1*<sup>-/-</sup>) mice. The number of bacteria in WT and RIPK3<sup>-/-</sup> alveolar M $\phi$  was identical before transfer (**Supplementary Figure 5E**). However, 4 weeks after adoptive transfer, the pulmonary bacterial burden was significantly lower in *Rag1*<sup>-/-</sup> mice that received *Mtb*-infected RIPK3<sup>-/-</sup> M $\phi$  than in the recipients of *Mtb*-infected WT M $\phi$  (**Figure 7e**). This experiment demonstrates that transfer of infected RIPK3<sup>-/-</sup> M $\phi$ , which are resistant to necrosis restrict bacterial replication independent of adaptive immunity *in vivo*. Thus RIPK3 plays an important role in early M $\phi$  immunity and protection against *Mtb* infection.

#### DISCUSSION

*Mtb* hijacks M $\phi$  cell death pathways to maintain an environment for propagation within the host. We and others have previously demonstrated that *Mtb* actively inhibits apoptosis, which has a protective role in both innate and adaptive immunity to *Mtb* infection.<sup>44</sup> By inducing necrosis, virulent *Mtb* is able to exit the M $\phi$  and escape anti-mycobacterial defense mechanisms.<sup>1</sup> Although we have shown that *Mtb* induces necrosis by targeting the mitochondrial inner membrane<sup>10,11,40</sup> and plasma membrane repair mechanisms,<sup>3</sup> the molecular mechanisms involved in necrosis remain largely unknown. Here we have extended these studies and shown that Bcl-x<sub>L</sub> and RIPK3 are involved in triggering M $\phi$  programmed necrosis during infection with virulent *Mtb*.

Recently a novel form of necrosis, necroptosis, was described, which depends on the action of a cytosolic complex containing RIPK1 and RIPK3. Formation of this complex is inhibited by the RIPK1 inhibitor necrostatin-1.<sup>17</sup> However, similar to another infection model,<sup>45</sup> we found no effect of RIPK1 on necrosis either by using a necroptosis inhibitor, necrostatin-1, or silencing RIPK1 (data not shown). As necroptosis seems to be independent of the mitochondria and is a rapid early event,<sup>46</sup> the mechanisms involved in the *Mtb*-induced necrosis, which develops slowly and reaches its maximum between 72 and 96 h after infection, might be different from classical necroptosis. Interestingly, a recent study suggests that induction of necroptosis by RIPK3 requires inactivation of caspase-8.<sup>47</sup> Similarly, our findings indicate that caspase 8 determines the fate of M $\phi$  infected with virulent *Mtb*. Following infection with *Mtb*, RIPK3 translocates from the cytosol to the mitochondria of M $\phi$ . Bcl-x<sub>L</sub>, an inhibitor of BAK<sup>27,28</sup> leading to a block of



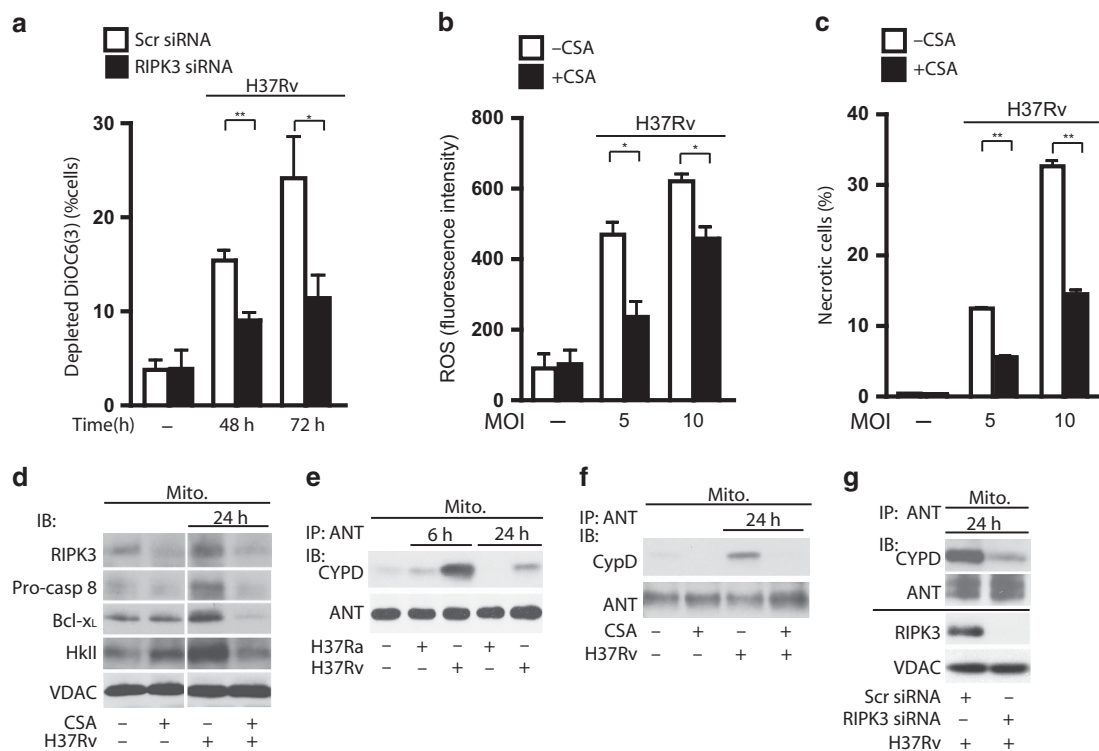


**Figure 5** RIPK3 induces CypD-dependent MPT in H37Rv-infected M $\phi$ . (a) M $\phi$  were transfected with RIPK3 or scrambled (Scr) control siRNA and were then infected with H37Rv (MOI 10). Cationic dye (DiOC6<sub>(3)</sub>) release from mitochondria (a measure for MPT) was measured at 48 and 72 h after infection. (b and c) Inhibition of CypD reduces ROS-dependent necrosis. (b) Equal numbers of CsA-treated (5  $\mu$ M) and untreated M $\phi$  were infected with H37Rv (MOI 5 or 10). After 48 h of infection ROS accumulation (b) was measured by FACS analysis using the fluorescent dye CM-H<sub>2</sub>XRos and cell viability (c) was determined using the Live-Dead Assay. (d) CypD inactivation reduces translocation of RIPK3, pro-caspase 8, Bcl-x<sub>L</sub> and HKII to the mitochondria in H37Rv-infected M $\phi$  at 24 h. Equal amounts of mitochondria from H37Rv-infected M $\phi$  treated with or without CsA (5  $\mu$ M) were subjected to Western blot analysis for RIPK3, pro-caspase 8, Bcl-x<sub>L</sub> and HKII after 24 h of infection. (e) Mitochondria from H37Ra or H37Rv infected M $\phi$  were subjected to IP with anti-ANT ab and were then subjected to western blot analysis for CypD. (f) CypD-ANT interaction is augmented in H37Rv-infected M $\phi$  and is inhibited by inactivation of CypD with CsA (5  $\mu$ M). (g) Top panel: RIPK3 is required for CypD-ANT interaction on the mitochondria. After 24 h of infection, mitochondria from H37Rv-infected M $\phi$  transfected with RIPK3 or scrambled (Scr) control siRNA were subjected to IP with anti-ANT ab and were then analyzed by Western blot for CypD. ANT was used as a loading control. Bottom panel: Silencing efficiency of RIPK3 siRNA. VDAC was used as a loading control. Results are expressed as mean  $\pm$  s.e., using nonparametric Student *t*-test. \*, Values of *P* < 0.05 were considered to be significant. Data are representative of three independent experiments. FACS, fluorescence-activated cell sorting.

caspace 8 activation and apoptosis,<sup>48</sup> protects RIPK3 from caspase 8-dependent proteolysis.<sup>19</sup> We also found that mitochondrial Bcl-x<sub>L</sub> is required for RIPK3 to prevent caspase 8 activation and inducing necrosis in *Mtb*-infected M $\phi$ . Although binding of Bcl-x<sub>L</sub> to caspase 8 was reported earlier,<sup>48</sup> we failed to find any binding of Bcl-x<sub>L</sub> to pro-caspase 8 (data not shown).

Although in the current study, we have not demonstrated how caspase 8 translocates into mitochondria, other studies have shown that in human lymphoblastoid cell lines caspase 8 was associated with cardiolipin rafts at contact points of the inner and outer mitochondrial membranes leading to its activation. Cardiolipin was also found to be responsible for the translocation of caspase 8 to the mitochondria as well as caspase 8 activation following death receptor signaling.<sup>49</sup> Targeting of tBid to the mitochondria and mobilization of cytochrome c are also cardiolipin dependent indicating their importance in the transduction of the apoptotic signaling cascades.<sup>50</sup>

Consistent with these studies we found that in M $\phi$  infected with an avirulent strain of *Mtb*, H37Ra, pro-caspase 8 is proteolytically processed, which not only correlates with

activation of the effector caspases 9 and 3 leading to apoptosis, but also with preventing necrosis by inactivation of RIPK3. We currently do not know the exact mechanism of mitochondrial caspase 8 activation in M $\phi$  infected with an avirulent strain of *Mtb*. Interestingly, Niture and colleagues<sup>51</sup> have reported that the levels of Bcl-x<sub>L</sub> on the mitochondria are regulated by a member of the phosphoglycerate mutase family 5 (PGAM5), which forms a bridge between Bcl-x<sub>L</sub> and Kelch-like ECH-associated protein-1 (a sensor of chemical and radiation-induced stress) and targets Bcl-x<sub>L</sub> degradation by activating an E3 ubiquitin ligase. The involvement of this or additional mechanisms in Bcl-x<sub>L</sub>-degradation or the role of signaling platforms, such as cardiolipin that promotes mitochondria-dependent caspase 8 activation remains to be determined. In addition, it is currently unclear whether Bcl-x<sub>L</sub> is the only anti-apoptotic component on the mitochondria involved in this mechanism. It is likely that other Bcl-2 family members including Mcl-1 and Bcl-2<sup>52,53</sup> may also contribute to RIPK3 mediated caspase 8-inactivation in mitochondria leading to the induction of necrosis.

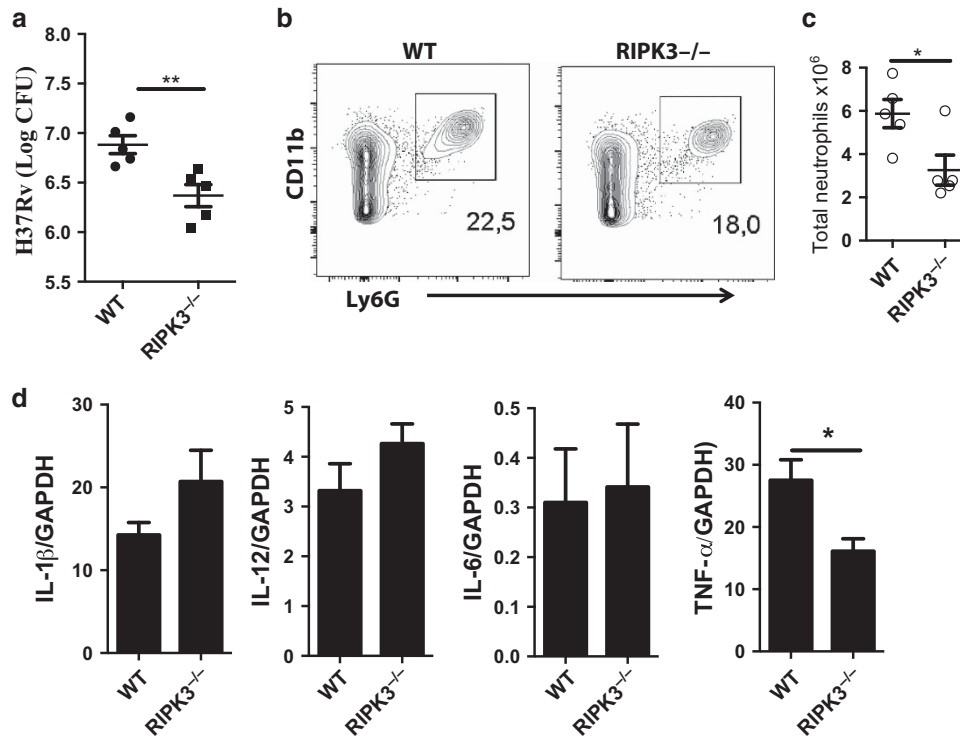


**Figure 6** Reduced bacterial burden in the lungs of RIPK3<sup>-/-</sup> mice infected with high dose of *Mtb*. (A) RIPK3<sup>-/-</sup> mice were infected with *Mtb* ( $1 \times 10^6$  CFU) through intravenous injection. After 4 weeks of infection, mice were sacrificed to quantify (a) bacterial load in the lungs. (b) Lung cells were immunophenotyped to assess recruitment of neutrophils by gating CD11b<sup>+</sup>Ly6G<sup>+</sup> cells. (c) Total number of neutrophils in the lungs of infected mice. (d) After 4 weeks of infection, the level of expression of cytokines in the lungs of infected animals (IL-6, TNF- $\alpha$ , IL-12, IL-1 $\beta$ ) was determined at mRNA level using qPCR. Results are expressed as mean  $\pm$  s.e., using nonparametric Student *t*-test. \*,\*\* Values of  $P < 0.05$  and  $P < 0.01$  were considered to be significant, respectively.

The mitochondria are a major source of energy and ROS production, and disruption of mitochondrial function significantly contributes to ROS generation and cell death. For example, blocking ROS accumulation in L929 cells prevents necrosis.<sup>26</sup> Our results indicate that in M $\phi$  infected with virulent *Mtb*, increased ROS accumulation contributed to induction of necrosis. Virulent *Mtb* may induce necrosis by several mechanisms including inhibition of ATP production, e.g., due to blocking of mitochondrial ADP transport by ANT,<sup>54</sup> sustained JNK activation<sup>55</sup> and release of toxic proteins from the permeable mitochondria.<sup>56</sup>

In cells with increased glucose consumption, NADH levels are drastically increased, which can result in increased accumulation of ROS.<sup>39</sup> Our results indicate that increased ROS accumulation in H37Rv-infected M $\phi$  requires activation of two independent mechanisms associated with mitochondria. First, the generation of sufficient amounts of electron donors and increased HKII levels on the mitochondria lead to enhanced production of glucose-6-phosphate, the rate-limiting step of glycolysis.<sup>25</sup> HKII is predominantly associated with VDAC on the mitochondria and couples oxidative phosphorylation to glycolysis, which is essential for ROS production. Thus reduction of mitochondrial HKII downregulates glycolysis as well as ROS generation. Interestingly, similar to H37Rv-infected M $\phi$ , HKII is highly upregulated on the mitochondria of many tumors, which leads to increased aerobic glycolysis

known as the Warburg effect.<sup>25,57</sup> Second, RIPK3 induces MPT, which interrupts the electron chain in mitochondrial complex I leading to electron-leakage and allows molecules with a size up to  $\sim 1.5$  kDa to exit the mitochondrial matrix. MPT is part of a cellular suicide mechanism and its contribution to the pathophysiology of several diseases including heart injury<sup>14</sup> is well documented. Although it was proposed that induction of MPT is a mechanism by which aging mitochondria are earmarked for removal, there is no evidence of this mechanism in studies using CypD knockout mice.<sup>15</sup> Thus the role of MPT under physiological conditions is still unclear. In contrast, under certain pathological conditions including M $\phi$  infection with virulent *Mtb*, MPT triggers induction of necrosis, which is essential for the release of the bacilli from the host cell ensuring the vicious cycle of infection. Here we have identified two different complementary mechanisms, MPT and HKII accumulation, which act in concert to increase ROS accumulation triggering a necrotic cell death program in *Mtb*-infected M $\phi$  (Figure 8).

How does RIPK3 induce MPT? Virulent *Mtb* increases HKII binding to VDAC on the outer mitochondrial membrane that enhances the generation of glucose-6-phosphate as well as CypD binding to the ANT<sup>58</sup> in the inner mitochondrial membrane. This opens the permeability transition pore causing MPT.<sup>15</sup> CypD keeps the MPT pore in the mitochondrial inner membrane in the “open” position by binding to ANT.<sup>59</sup> Here

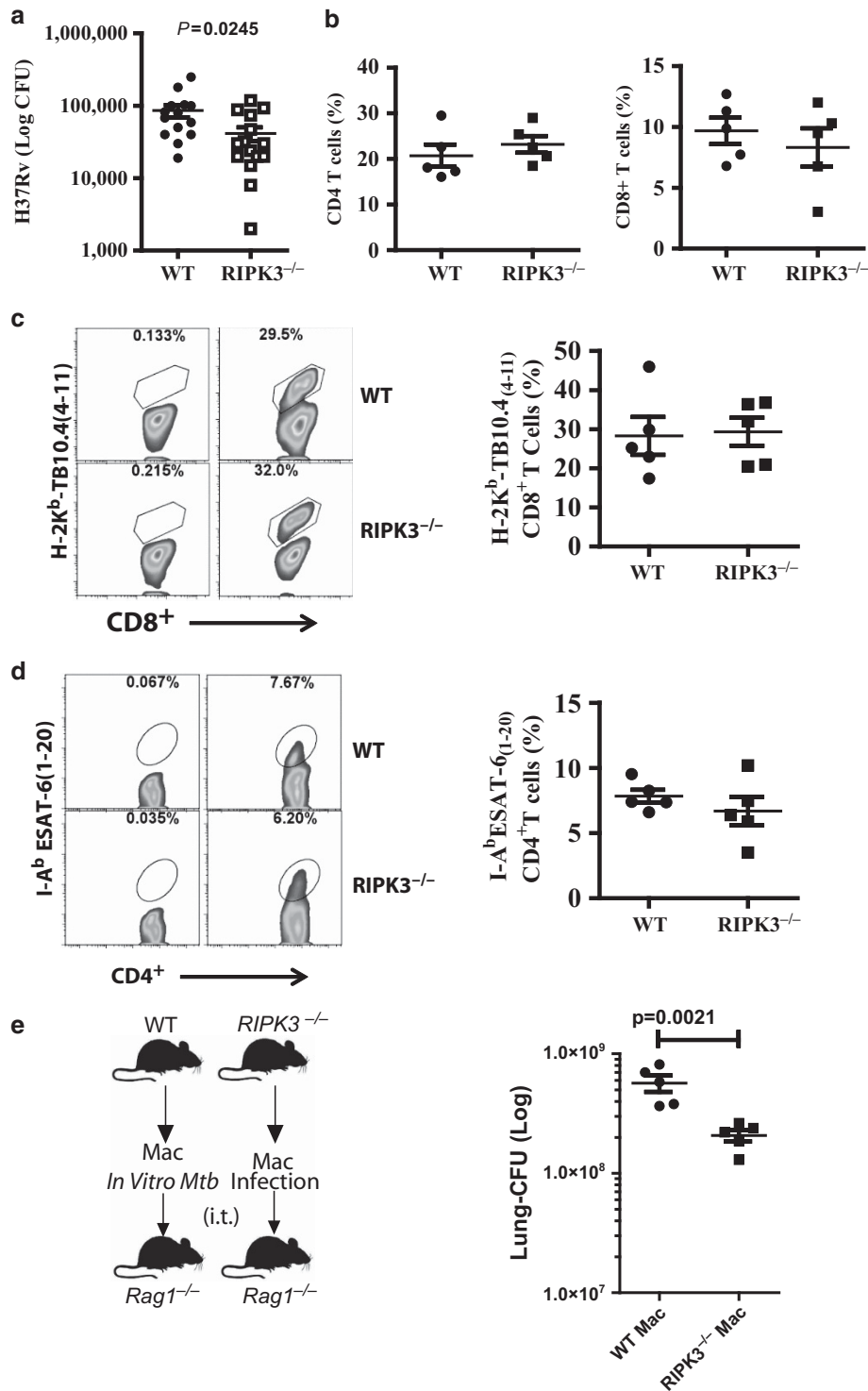


**Figure 7** RIPK3-deficient M $\phi$  mediate host resistance to pulmonary *Mtb* infection. (a) Bacterial burden in the lung after 5 weeks of aerosolized *Mtb* infection (H37Rv, 50–100 CFU) was significantly lower in RIPK3<sup>-/-</sup> mice compared with WT mice. The data were pooled from two independent experiments. (b) After 5 weeks of *Mtb* infection the frequency of CD3<sup>+</sup>CD4<sup>+</sup> T cells (left) and CD3<sup>+</sup>CD8<sup>+</sup> T cells (right) was determined in the lungs. (c and d) Representative flow cytometry plots of (c) TB10.4<sub>4-11</sub> MHC class I tetramer staining of CD8<sup>+</sup> T cells (d) IA<sup>b</sup>ESAT6<sub>1-20</sub> MHC class II tetramer staining of CD4<sup>+</sup> T cells and in the lungs 5 weeks post-*Mtb* infection. (e) The anti-necrotic properties of *Mtb*-infected RIPK3<sup>-/-</sup> M $\phi$  reflect the innate control of infection *in vivo*. Bacterial burden in the lung 4 weeks after intratracheal (i.t.) transfer of H37Rv-infected RIPK3<sup>-/-</sup> or WT alveolar M $\phi$  into Rag1<sup>-/-</sup> mice. Results are expressed as mean  $\pm$  s.e. Data were analyzed using nonparametric Student *t*-test. \*, Values of  $P < 0.05$  were considered to be significant.

we show that CypD binds to ANT to induce MPT in virulent *Mtb*-infected-M $\phi$ . We furthermore demonstrate that RIPK3 is required for binding of CypD to ANT to initiate ROS-mediated necrosis. Considering that several components of MPT are kinase substrates<sup>60</sup> it is tempting to speculate that RIPK3 may phosphorylate some components involved in MPT for generating increased levels of ROS.

RIPK3<sup>-/-</sup> mice were more resistant than WT mice in both the low-dose aerosol and high-dose intravascular models of *Mtb* infections. In addition, we observed a significant decrease in the total number of neutrophils in the lungs of *Mtb*-infected RIPK3<sup>-/-</sup> mice. Reduced number of neutrophils further supports the notion of less necrosis in RIPK3<sup>-/-</sup> *Mtb*-infected animals. However, this protection was mainly dependent on M $\phi$  immunity, considering that there were no qualitative or quantitative differences in T-cell-mediated immunity between *Mtb*-infected RIPK3<sup>-/-</sup> or WT mice. In addition, M $\phi$  transfer experiments directly demonstrated that the fate of *Mtb*-infected M $\phi$  was the key determinant of the relative resistance of these mice. Interestingly, a recent study by Albert's group has elegantly shown that RIPK3-mediated necroptosis is more effective in cross-priming T cells than apoptosis.<sup>20</sup> However, we speculate that during *Mtb* infection the host may compensate for the lack of necrosis-dependent T-cell-mediated immunity via apoptosis to maintain an adequate T-cell-response to *Mtb* infection.<sup>5-7</sup> The links between apoptotic/necrotic M $\phi$ , DC, and T-cell immunity in the control of *Mtb* infection certainly requires further investigation.

The dramatic differences in behavior of avirulent vs. virulent strains of *Mtb* in induction of apoptosis and necrosis, respectively, suggest the involvement of a specific pathogen-encoded inducer of RIPK3-dependent necrosis, which needs to be elucidated. Several virulent strains of *Mtb* encode specific genes, such as the *nuoG* gene, which actively inhibits the apoptotic death pathway in M $\phi$ .<sup>61</sup> The *nuoG* gene of *Mtb* encodes type I NADH dehydrogenase, which neutralizes NOX-2 dependent ROS production in the M $\phi$  and is required for induction of apoptosis.<sup>62</sup> It will be interesting to know whether the *nuoG* gene or other genes are involved in RIPK3-dependent necrosis.

There are several differences between our study and other previous published data using various cell lines including HeLa, 293A, L929, and 3T3-cells.<sup>26,46,63,64</sup> We envision that these differences are mainly due to using cell lines and soluble ligands vs. primary M $\phi$  and live-replicating bacteria. For instance, addition of caspase inhibitors to L929 cells induces necrosis due to autocrine production of TNF in the absence of active pro-apoptotic caspases.<sup>35</sup> In contrast, addition of caspase inhibitors to primary human M $\phi$  in the absence of *Mtb* infection does not induce necrosis as autocrine TNF-production is minimal indicating that the pathways leading to necrosis in certain cell lines and in primary M $\phi$  are significantly different. Similar to our findings in human M $\phi$  infected with virulent *Mtb*, Roca and Ramakrishnan have reported a comparable role of RIPK3 in a zebra fish model of infection with *Mycobacterium marinum*,<sup>65</sup> which underscores the evolutionary conservation

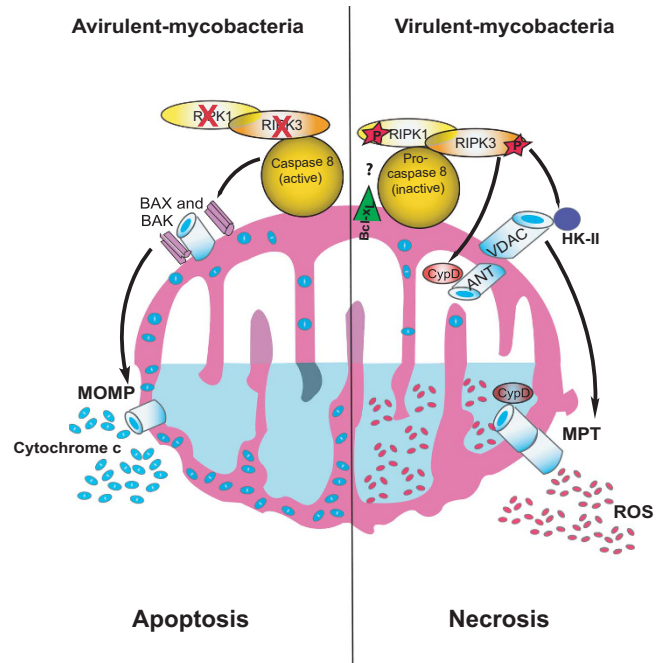


**Figure 8** Model of RIPK3-dependent programmed necrosis and caspase 8-dependent apoptosis in M $\phi$  infected with *Mtb*. In M $\phi$  infected with virulent *Mtb* cytosolic RIPK3 and pro-caspase 8 translocate to the mitochondria. In the presence of Bcl-x<sub>L</sub>, RIPK3 is activated that enhances binding of HKII to VDAC on the outer mitochondrial membrane. At the same time activated RIPK3 triggers CypD-dependent formation of the MPT pore via interaction between ANT and VDAC leading to leakage of the electron chain. Both mechanisms seem to be required for increasing ROS-dependent necrosis (right). In M $\phi$  infected with avirulent *Mtb* the RIPK3 and caspase 8 also translocate to the mitochondria but this step is quickly followed by activation of caspase 8 and degradation of RIPK3. Oligomerization of BAX and BAK, which in turn allows the release of pro-apoptotic molecules (e.g., cytochrome c) leads to apoptosis (left). The exact action mechanism of Bcl-x<sub>L</sub> function is still unknown.

of the RIPK3-dependent necrosis pathway in *Mtb* pathogenesis.

Despite the world-wide application of BCG vaccination and other anti-*Mtb* interventions, *Mtb* remains one of the most successful human pathogens. More than 2 billion people carry latent tuberculosis infection, and ~20 million people have currently active tuberculosis, of which 1.8 million people die every year.<sup>66</sup> The success of this pathogen is closely linked to its ability to alter the intracellular environment of M $\phi$  including induction of cell death. Thus dissecting the molecular mechanisms involving mitochondria as entities determine whether *Mtb*-infected M $\phi$  undergo apoptosis or necrosis is of significant importance in identifying the outcome of host immunity to *Mtb* infection and might pave the road for novel therapies that target the necrotic death program.

## METHODS

**Materials.** Anti-caspase 8 (551242), and anti-RIP1 (551042) antibodies were from BD Biosciences. Anti-caspase 8 (52183, for immunofluorescence), anti-RIPK3 (56164), and anti-adenine nucleotide translocase (ANT, 109864) antibodies were from Abcam. Anti-CypD (AP1035) antibody was from Calbiochem (Merck KGaA,



Darmstadt, Germany). Anti-hexokinase II (2106), anti-BAX (2772), anti-Bcl-x<sub>L</sub> (2762), anti-caspase 3 (9662), anti-caspase 9 (9502), anti-BID (2002), anti-GAPDH (2118), and anti-caspase 8 (Asp387, 14071, for flowcytometry) were from Cell Signaling Technology (Danvers, MA). Anti-VDAC (SP5361P) antibody was from Acris (Herford, Germany). Active caspase 3 for flowcytometry was from BD. Anti-human mitochondria antibody (HMS-0100) was from Immunovision. Dylight 650-conjugated Donkey anti-rabbit IgG antibody and Alexa fluoro 488-conjugated Donkey anti-human IgG antibody were from Jackson Immuno Research Laboratory (Bar Harbor, ME, USA). The caspase inhibitor z-IETD-FMK (FMK007) was from R&D Systems (Minneapolis, MN). Gammabind protein G sepharose (17-0885-01) was from GE Health Care (Pittsburgh, PA). Cyclosporin A (30024), Tiron (89460) and Protease Inhibitor Cocktail (P2714) from Calbiochem (Saint Louis, MO) and Phosphatase Inhibitor Cocktail 1 (P2850) was from Sigma-Aldrich (St. Louis, MO). Mitochondria/Cytosol Fractionation Kit (ThermoFisher Scientific Mitochondrial Isolation kit #89874, Rockford, IL) and MitoTracker Red CMXRos (M7512), MitoTracker Red CM-H<sub>2</sub>XRos (M7513), and LIVE/DEAD Fixable Dead Cell Stain Kits (MP34955) from Invitrogen (Eugene, OR).

**In vivo *M. tuberculosis* infection.** Six- to ten-week-old C57BL/6 or *Rag1*<sup>-/-</sup> mice were obtained from Jackson Labs; *RIPK3*<sup>-/-</sup> mice were obtained from Genentech. Mice were infected with virulent *M. tuberculosis* (H37Rv) via the aerosol route using a nose-only exposure unit and received ~50–100 CFU/mouse<sup>67</sup> or intratracheally (0.5 × 10<sup>6</sup> CFU) or intravenously (1 × 10<sup>6</sup> CFU)<sup>3</sup>. Mice were killed by CO<sub>2</sub> inhalation and the lung, spleen, and lymph node were aseptically removed, minced, and pressed through 70-μl cell strainer followed by red blood cell lysis to obtain single-cell suspension. Bronchoalveolar lavage was performed with phosphate-buffered saline (PBS) in mice infected intratracheally.<sup>3,8</sup>

**Adoptive transfer models of infection.** Alveolar Mφ were collected from the BAL of naive WT and *RIPK3*<sup>-/-</sup> mice and were immediately suspended at a concentration 0.5 × 10<sup>6</sup> cells/500 μl RPMI medium with 10% fetal calf serum and infected in suspension using virulent H37Rv (MOI ~ 1) for 30 minutes. Free bacteria were then removed by 6 washes with cold PBS, each time followed by centrifugation for 10 min at 1000 RPMI at 4 °C. Cells were resuspended in PBS at 0.5 × 10<sup>6</sup>/40 μl and transferred by the intratracheal route into naive C57BL/6 mice.<sup>3,5</sup>

**CFU determination.** Following infection, mice were killed and their lungs removed and individually homogenized in 0.9% NaCl-0.02% Tween 80 with a Mini-Bead-Beater-8 (BioSpec Products) (Bartlesville, OK). Viable bacteria were enumerated by plating 10-fold serial dilutions of organ homogenates onto 7H11 agar plates (Thermo Fisher Scientific Remel Products, Lenexa, KS). Colonies were counted after 3 weeks of incubation at 37 °C.

**Bacteria.** The virulent *Mtb* strain H37Rv and attenuated stain H37Ra (American Type Culture) were grown in Middlebrook 7h9 broth (BD Biosciences, Sparks, MD) with BBL Middlebrook OADC Enrichment (Becton Dickson, Sparks, MD) and 0.05% (vol/vol) Tween 80 Difco (Sparks). Aliquots were distributed into small tubes and stored at –80 °C. 100 μl of the aliquot was serially diluted 10-fold with 0.02% Tween 80 in PBS and plated on 7H11 agar plates (Thermo Fisher Scientific Remel Products, Lenexa, KS, USA). The bacterial concentration of each batch was determined by colony counting after 4-weeks.

**Cells and cell culture.** Human mononuclear leukocytes from buffy coat preparations (Research Blood Component, Boston, MA, USA) were cultured for 7 days in Iscove's modified Dulbecco's medium (IMDM) containing 10% (vol/vol) human AB serum (Gemini bio-Products, West Sacramento, CA) at a density of 2.0 × 10<sup>6</sup> cells per ml in six-well plates and 2.0 × 10<sup>7</sup> cells per ml in 10 cm plates, and then

were changed to IMDM with 2% (vol/vol) human AB serum 1 day before challenged with varying MOI of *Mtb*. Bone marrow from 8- to 10-week-old mice was harvested from femurs and differentiated into Mφ for 7 days in RPMI-1640 (Invitrogen) supplemented with 10% L929 cell (ATCC)-conditioned medium, 10% fetal bovine serum, 2 mM L-glutamine and 1 mM sodium pyruvate, 1% essential and non-essential amino acids (Invitrogen), 100 U/ml penicillin and 100 μg/ml streptomycin.

**In vitro infection.** Adherent human Mφ were infected with H37Rv or H37Ra at different MOIs. After 4 h the Mφ were washed three times with HBSS to remove non-adherent bacilli and replaced with fresh IMDM with 2% AB. Adherent murine Mφ were infected with H37Rv at different MOIs. After 4 h the Mφ were washed three times with warm PBS to remove non-adherent bacilli and replaced with fresh media containing fetal bovine serum.

**FACS analysis.** Cells were stained as previously described using antibodies specific for mouse CD3, CD4, CD8, and CD19 (BD Biosciences) Ly6G, Ly6c, CD11b, F4/80, CD11c (San Diego, CA).<sup>5</sup> Antigen-specific CD4<sup>+</sup> and CD8<sup>+</sup> T cells were identified using IA<sup>b</sup>ESAT<sub>6,20</sub> and H2-K<sup>b</sup>TB10.4<sub>4-11</sub> tetramers, respectively (National Institutes of Health Tetramer Core Facility, Emory University Vaccine Centre, Atlanta, GA, USA). Cleaved Caspase 8 Staining was performed in WT and *RIPK3*<sup>-/-</sup> Mφ. Cells were washed, collected and suspended in formaldehyde to obtain a final concentration of 4% for 30 min at room temperature. Cells were permeabilized by adding ice-cold 100% methanol slowly to pre-chilled cells, while gently vortexing, to a final concentration of 90% methanol by incubating 30 min on ice. Cells were washed by with buffer and PE-conjugated cleaved caspase 8 Ab was added for 1 h at room temperature. Cells were then washed and resuspended in buffer to be analyzed by flow cytometer. Flow cytometry was performed by using a BD LSR-II (BD Biosciences) and FlowJo analysis software (Tree Star, Ashland, OR).

**In vitro T cell proliferation.** CD3<sup>+</sup> T cells were purified from spleens of naive WT and *Annex1*<sup>-/-</sup> mice using MACS column purification procedure by negative selection (Pan T cell kit—MACS Miltenyi). The purity of CD3<sup>+</sup> T cells was usually between 92–97%. Purified CD8<sup>+</sup> T cells were stained with 5 μM CFSE in PBS containing 0.1% bovine serum albumin at room temperature. Staining was stopped after 8 min of incubation by addition of RPMI medium containing 10% fetal bovine serum. T cells were then cultured with different concentrations of anti-CD3 and anti-CD28. After 3 days, T cell proliferation was measured by reduction in CFSE expression (CFSE<sup>low</sup>) using flow cytometry.

**ELISPOT assay.** The IFN-γ Elispot assay was conducted according to the manufacturer's instructions (R&D Systems). Briefly, isolated cells were seeded into a 96-well plate pre-coated with mouse IFN-γ capturing Abs. Cells were then incubated for 24 h with or without antigenic stimulation. The plate was developed and the spots were enumerated using a series A immunospot plate reader, Image Acquisition version 4.0, and Immunospot version 3.2 analysis software (Cellular Technology, Cleveland, OH).

**Isolation of mitochondria from Mφ.** Mitochondria were isolated using the Mitochondria/Cytosol Fractionation Kit (ThermoFisher Scientific Mitochondrial Isolation kit #89874) according to the manufacturer's recommendations. Briefly, cells were washed twice with ice-cold PBS and then 1 ml of Isotonic Mitochondrial Buffer (containing protease inhibitors) was added. Cells were homogenized on ice by passing through a 25-gauge needle (Becton Dickinson) after detachment from the culture dish by using a cell scraper. The lysate was centrifuged at 600 × g for 10 min at 4 °C to remove the nuclei, debris and intact cells. The supernatants were centrifuged at 10 000 × g for 30 min at 4 °C. The enriched mitochondrial fraction was washed and lysed in 100 μl of a buffer containing Tris-HCl (50 mM, pH7.4), NaCl (150 mM), EDTA (5 mM), Triton X-100 (1%), sodium ortho-vanadate (0.2 mM) and protease

inhibitor cocktail (Sigma) at 4 °C and stored at -80 °C together with the cytosolic fraction. The purity of the mitochondria was determined by taking 10 µg of protein from the mitochondrial and cytosolic fractions and measuring Bcl-x<sub>L</sub> and GAPDH levels by Western blotting.

**Silencing of the genes encoding human RIPK3, Bcl-x<sub>L</sub>, hexokinase II, MLKL and BAX.** The target siRNA sequences for human RIPK3 specific siRNA (5'-GGAAUGCCUACCAAAAACU-3'), the Bcl-x<sub>L</sub> siRNA (5'-GGAGAUGCAGGUAUUGGUG-3'),<sup>68</sup> and for hexokinase II (5'-CACGAUGAAUUGAACCUGG-3'),<sup>69</sup> MLKL siRNA is a pool of 3 different duplexes (5'-GGAAUACCGUUUCAGAUUGtt-3', 3'-ACAUCUGAAACGGUAUUCct-5'; 5'-GGAAUAGUGAGGUUCACU Ut-3', 3'-AAGUGAACCCUCACUAUUCct-5'; 5'-GAAGGCUGU GAUUCUAAGAt-3', 3'-UCUUGAUAACACGCCUUCt-5') and RIPK3 second siRNA pool (5'-CUGAGUGGCUAAAACAAACUtt-3', 3'-AGUUUGUUAGCCACUCAt-5'; 5'-GGAGACAACAACUACU UGtt-3', 3'-UCAAGUAGUUUGUCUCct-5'; 5'-CUCCAAGA-GUUACGAGUUt-3', 3'-UAACUCGUAACUCUUGGAGtt-5') were generated by IDT. Human BAX-specific siRNA (#6321) was from Cell Signaling Technology. Mφ were cultured in IMDM with 10% (vol/vol) human AB serum and in IMDM with 2% human AB serum 1 day before transfection. All siRNA was transfected at 37 °C into the cells at a final concentration of 50 nM with Lipofectamine RNAiMAX (13778-150, Invitrogen, Waltham, MA). Mφ were infected with *Mtb* 48–72 h after transfection.

**Immunoblot analysis.** Protein was measured with the Bradford assay. Samples (5 µg) were fractionated by SDS-polyacrylamide gel electrophoresis and protein was transferred to a PVDF membrane at 4 °C. The membrane was blocked with 5% dried milk in Tris HCl buffer (10 mM), pH 8.0 containing NaCl (150 mM) and Tween 20 (0.5%) and was incubated with the appropriate primary antibodies overnight at 4 °C. After three washes blots were incubated with the corresponding horseradish peroxidase-conjugated secondary antibodies for 1 h at room temperature. Enhanced chemiluminescence reagent was added and the blots were exposed to Denville Hyblot CL film (Holliston, MA). Western input of Mφ infected with H37Rv for RIPK3, RIPK1, procaspase8, and loading control (actin and VDAC) is incorporated in supplementary (Supplementary Figure 3A).

**Co-immunoprecipitation.** After centrifugation at 18 000 × g for 30 min the Mφ lysates were immunoprecipitated overnight with immobilized monoclonal antibody under gentle rotation at 4 °C. 50 µl of protein G beads-slurry (50%) was added to the sample and the mixture incubated for another 1 h at 4 °C. To remove non-specific bound material the beads were washed with lysis buffer 3 times. The beads were then gently mixed with lysis buffer, centrifuged at 4 °C and the supernatant removed. Twenty µl of SDS-sample buffer was added to the samples and the samples were then loaded on SDS-polyacrylamide gel electrophoresis gels after boiling.

**Assessment of MPT.** MPT was measured as described.<sup>11</sup> Briefly, human Mφ were cultured at a density of 1.5 × 10<sup>6</sup> mononuclear cells per well with 2 ml medium containing IMDM with 2% AB serum in six-well cluster plates (Corning Glass, Corning, New York). After 7 days cells were pre-loaded with 1.5 nM DiOC<sub>3</sub> in IMDM for 20 min at 37 °C, washed, and incubated at 37 °C for 10 min in medium containing 15 µg/ml digitonin, washed, and fixed with 1% paraformaldehyde for 1 h at r.t. Mφ were then dislodged with a rubber policeman, washed with PBS and resuspended in PBS with 1% (wt/vol) bovine serum albumin. A FACSort flow cytometer (BD Biosciences) was used for flow cytometry.

**Assay for apoptosis.** Apoptosis was measured by determining caspase 3-activation using western blotting and flow cytometry because the caspases 3/10 are the direct executioners of pro-apoptotic pathways. Apoptosis was also determined by flow cytometry with Annexin V staining. Briefly, RIPK3<sup>-/-</sup> Mφ were infected with H37Ra (MOI 5) for 4 h followed by washing and incubation for 96 h in BMDM media. Cells were harvested and incubated with Annexin V dye in

buffer recommended by manufacturer for 30 min. Mφ were resuspended with 7AAD for dead cell staining and acquired using flowcytometer within 1 h.

**Assay for necrosis.** Mφ necrosis was evaluated *in vitro* and *in vivo* by flow cytometry with the LIVE/DEAD fixable Dead Cell Stain kit (Invitrogen, L34955) according to the instructions of the manufacturer. Briefly, adherent infected and uninfected human Mφ (1.5 × 10<sup>5</sup> per well) were washed, 0.5 ml of 1% of reconstituted fixable violet fluorescent reactive dye was added and the mixture incubated at room temperature for 30 min in dark. Mφ were washed and fixed with 3.7% paraformaldehyde for 1 h at room temperature. Mφ were dislodged with a rubber policeman, washed and resuspended in PBS with 1% bovine serum albumin. A FACSort flow cytometer was used for flow cytometry. In some experiments necrosis was measured with cell death detection ELISA<sup>PLUS</sup> photometric enzyme immunoassay (11 920685 001; Roche Applied Science, Sandhofer Strasse, Mannheim, Germany).

**ROS assay.** ROS accumulation was measured by using reduced rosamine-Mitotracker probes (Invitrogen, M7513). Adherent Mφ were washed with IMDM medium, stained with 200 nM Mitotracker Red CM-H<sub>2</sub>XRos in IMDM without serum at 37 °C for 30 min. Then the medium was removed, and the cells were washed and fixed with 3.7% paraformaldehyde for 1 hour at room temperature. After fixation, Mφ were washed and resuspended in 0.5 ml PBS with 1% bovine serum albumin. Fluorescence intensity of ROS was measured using a flow cytometer. To control for possible changes in the mitochondrial mass under the different conditions the cells were tested with the ROS-insensitive mitotracker dye red FM (Invitrogen). No differences in fluorescence emission were seen indicating that the mitochondrial mass was not different in the Mφ subjected to the different experimental conditions.

**NADH determination.** NADH in Mφ extracts was measured with the NAD<sup>+</sup>/NADH Quantification Colorimetric Kit from BioVision (Milpitas, CA) according to the recommendation of the manufacturer.

**Immunostaining and confocal microscopy.** Mφ were cultured on poly-D lysine-coated cover slips in 24-well plates at a density of 1.5 × 10<sup>5</sup> cells/well and were infected for 24 h with mCherry labeled H37Rv. Mφ were then fixed for 1 h with 4% paraformaldehyde and blocked overnight at 4 °C with PBS containing 10% horse serum. Cover slips were incubated for 2 h at room temperature with anti-mitochondria, anti-caspase 8 or anti-RIPK3 (dilution, 1:100) ab. Mφ were then washed and stained for 1 h at room temperature with fluorescent secondary ab. Mφ were mounted and then subjected to confocal and transmission light microscopy. Microscope images were acquired at the Brigham and Women's Confocal Core Facility with a Nikon TE2000-U inverted microscope, Nikon C1 Plus confocal system, 60 × Nikon Plan Apochromat objective, 10-mW Spectra Physics 488-nm argon laser, Melles Griot Red HeNe 543-nm laser, Chroma 515-nm/30-nm and 543-nm emission filters and a 30-µm pinhole. Images were acquired under identical exposure conditions and micrographs were compiled and analyzed with Nikon EZ-C1 v3.8 (Nikon, Minato, Tokyo, Japan) and Adobe Photoshop v10.0.1. Colocalization of RIPK3 and pro-caspase 8 on the mitochondria was quantified using Metamorph. Each channel (R, G, B) was considered separately with each pixel assigned an intensity value (0–255) with care taken to assure that no pixel was oversaturated in any image used for quantification. The lower threshold is set whereby areas of the image without staining are excluded. The software then calculates that area of caspase 8 or RIPK3 with mitotracker and reports it in terms of percent positive cells. Quantification was done on 100–200 cells for every condition, and representative images are shown from at least three independent experiments.

**Quantitative real-time PCR.** Total RNA was isolated with Trizol reagent from lungs of *Mtb*-infected animals. RNA was quantified with the help of a NanoDrop spectrophotometer (Wilmington, DE). The

A260/A280 ratio of all samples was in the range of 1.90 to 2.00. DNA contamination from RNA samples was removed by amplification grade DNase (Ambion Invitrogen; according to manufacturer's instructions). Briefly, RNA samples (1 µg) were incubated with DNase (1 U) for 15 min in the reaction buffer. After the incubation, DNase activity was terminated by stop solution. Further, the samples were heated to 70 °C for 10 min to inactivate DNase activity. Real time PCR was performed using SYBR Green Master Mix Kit. Melting curve analysis was performed to eliminate the possibility of non-specific amplification. Results are represented in arbitrary units. Analysis was done by comparative Ct method, where Ct values were normalized against the house-keeping control GAPDH.

**Statistics.** Results are expressed as mean ± s.d. or s.e.m. The data were analyzed by using Microsoft Excel Statistical Software (Jandel, San Rafael, CA, USA) using the *t*-test for normally distributed data with equal variances. In some experiments, one-way analysis of variance with Dunnett's posttest or with Bonferroni's posttest was performed using Prism version 5 for Windows (Graph-Pad Software, La Jolla, CA).

**Ethics statement.** All animal experiments were conducted in accordance with Canadian Council on Animal Care guidelines. The animal used protocol was approved by the McGill Animal Care Committee (protocol number: 2010-5860).

**SUPPLEMENTARY MATERIAL** is linked to the online version of the paper at <http://www.nature.com/mi>

#### ACKNOWLEDGMENTS

We are grateful to V.W. Hsu, E Remold-O'Donnell and C Geadas for helpful discussions and Nancy Kedersha for supplying anti-mitochondrial antibody. This study was supported by the US National Institute of Health Grant AI072143 to H.G.R. and the Canadian Institute of Health Research (CIHR) Foundation Grant (FDN-143273) to M.D and M.D. holds a CIHR New Investigator Award.

#### DISCLOSURE

The authors declared no conflict of interest.

© 2017 Society for Mucosal Immunology

#### REFERENCES

- Behar, S.M., Divangahi, M. & Remold, H.G. Evasion of innate immunity by *Mycobacterium tuberculosis*: is death an exit strategy? *Nat. Rev. Microbiol.* **8**, 668–674 (2010).
- Chen, M. *et al.* Lipid mediators in innate immunity against tuberculosis: opposing roles of PGE2 and LXA4 in the induction of macrophage death. *J. Exp. Med.* **205**, 2791–2801 (2008).
- Divangahi, M. *et al.* *Mycobacterium tuberculosis* evades macrophage defenses by inhibiting plasma membrane repair. *Nat. Immunol.* **10**, 899–906 (2009).
- Martin, C.J. *et al.* Efferocytosis is an innate antibacterial mechanism. *Cell Host Microbe* **12**, 289–300 (2012).
- Divangahi, M., Desjardins, D., Nunes-Alves, C., Remold, H.G. & Behar, S.M. Eicosanoid pathways regulate adaptive immunity to *Mycobacterium tuberculosis*. *Nat. Immunol.* **11**, 751–758 (2010).
- Hinchey, J. *et al.* Enhanced priming of adaptive immunity by a proapoptotic mutant of *Mycobacterium tuberculosis*. *J. Clin. Invest.* **117**, 2279–2288 (2007).
- Winau, F., Kaufmann, S.H. & Schaible, U.E. Apoptosis paves the detour path for CD8 T cell activation against intracellular bacteria. *Cell. Microbiol.* **6**, 599–607 (2004).
- Tzelepis, F. *et al.* Annexin1 regulates DC efferocytosis and cross-presentation during *Mycobacterium tuberculosis* infection. *J. Clin. Invest.* **125**, 752–768 (2015).
- Green, D. & Kroemer, G. The central executioners of apoptosis: caspases or mitochondria?. *Trends Cell Biol.* **8**, 267–271 (1998).
- Gan, H., He, X., Duan, L., Mirabile-Levens, E., Kornfeld, H. & Remold, H.G. Enhancement of antimycobacterial activity of macrophages by stabilization of inner mitochondrial membrane potential. *J. Infect. Dis.* **191**, 1292–1300 (2005).
- Chen, M., Gan, H. & Remold, H.G. A mechanism of virulence: virulent *Mycobacterium tuberculosis* strain H37Rv, but not attenuated H37Ra, causes significant mitochondrial inner membrane disruption in macrophages leading to necrosis. *J. Immunol.* **176**, 3707–3716 (2006).
- Keane, J., Remold, H.G. & Kornfeld, H. Virulent *Mycobacterium tuberculosis* strains evade apoptosis of infected alveolar macrophages. *J. Immunol.* **164**, 2016–2020 (2000).
- Green, D.R., Galluzzi, L. & Kroemer, G. Mitochondria and the autophagy-inflammation-cell death axis in organismal aging. *Science* **333**, 1109–1112 (2011).
- Green, D.R. & Kroemer, G. The pathophysiology of mitochondrial cell death. *Science* **305**, 626–629 (2004).
- Baines, C.P. *et al.* Loss of cyclophilin D reveals a critical role for mitochondrial permeability transition in cell death. *Nature* **434**, 658–662 (2005).
- Nakagawa, T. *et al.* Cyclophilin D-dependent mitochondrial permeability transition regulates some necrotic but not apoptotic cell death. *Nature* **434**, 652–658 (2005).
- Tenev, T. *et al.* The Ripoptosome, a signaling platform that assembles in response to genotoxic stress and loss of IAPs. *Mol. Cell* **43**, 432–448 (2011).
- Vandenabeele, P., Declercq, W., Van, H.F. & Vanden, B.T. The role of the kinases RIP1 and RIP3 in TNF-induced necrosis. *Sci. Signal.* **3**, re4 (2010).
- Chan, F.K. *et al.* A role for tumor necrosis factor receptor-2 and receptor-interacting protein in programmed necrosis and antiviral responses. *J. Biol. Chem.* **278**, 51613–51621 (2003).
- Yatim, N. *et al.* RIPK1 and NF-κB signaling in dying cells determines cross-priming of CD8(+) T cells. *Science* **350**, 328–334 (2015).
- Kaczmarek, A., Vandenabeele, P. & Krysko, D.V. Necroptosis: the release of damage-associated molecular patterns and its physiological relevance. *Immunity* **38**, 209–223 (2013).
- Murphy, M.P. How mitochondria produce reactive oxygen species. *Biochem. J.* **417**, 1–13 (2009).
- Tretter, L. & Adam-Vizi, V. Inhibition of Krebs cycle enzymes by hydrogen peroxide: a key role of [α]-ketoglutarate dehydrogenase in limiting NADH production under oxidative stress. *J. Neurosci.* **20**, 8972–8979 (2000).
- Tretter, L. & Adam-Vizi, V. Alpha-ketoglutarate dehydrogenase: a target and generator of oxidative stress. *Philos. Trans. R. Soc. Lond. B Biol. Sci.* **360**, 2335–2345 (2005).
- Robey, R.B. & Hay, N. Mitochondrial hexokinases: guardians of the mitochondria. *Cell Cycle* **4**, 654–658 (2005).
- Cho, Y.S. *et al.* Phosphorylation-driven assembly of the RIP1-RIP3 complex regulates programmed necrosis and virus-induced inflammation. *Cell* **137**, 1112–1123 (2009).
- Willis, S.N. *et al.* Proapoptotic Bak is sequestered by Mcl-1 and Bcl-xL, but not Bcl-2, until displaced by BH3-only proteins. *Genes Dev.* **19**, 1294–1305 (2005).
- Edlich, F. *et al.* Bcl-x(L) retrotranslocates Bax from the mitochondria into the cytosol. *Cell* **145**, 104–116 (2011).
- Korsmeyer, S.J., Wei, M.C., Saito, M., Weiler, S., Oh, K.J. & Schlesinger, P.H. Pro-apoptotic cascade activates BID, which oligomerizes BAK or BAX into pores that result in the release of cytochrome c. *Cell Death Differ.* **7**, 1166–1173 (2000).
- Rodriguez, D.A. *et al.* Characterization of RIPK3-mediated phosphorylation of the activation loop of MLKL during necroptosis. *Cell Death Differ.* **23**, 76–88 (2016).
- Feoktistova, M. *et al.* cIAPs block Ripoptosome formation, a RIP1/caspase-8 containing intracellular cell death complex differentially regulated by cFLIP isoforms. *Mol. Cell* **43**, 449–463 (2011).
- Kim, S.J. & Li, J. Caspase blockade induces RIP3-mediated programmed necrosis in Toll-like receptor-activated microglia. *Cell Death Dis.* **4**, e716 (2013).
- Mcllwain, D.R., Berger, T. & Mak, T.W. Caspase functions in cell death and disease. *Cold Spring Harb. Perspect. Biol.* **5**, a008656 (2013).
- Salvesen, G.S. & Walsh, C.M. Functions of caspase 8: the identified and the mysterious. *Semin. Immunol.* **26**, 246–252 (2014).



35. Oberst, A. *et al.* Catalytic activity of the caspase-8-FLIP(L) complex inhibits RIPK3-dependent necrosis. *Nature* **471**, 363–367 (2011).
36. Kikuchi, J. *et al.* The novel orally active proteasome inhibitor K-7174 exerts anti-myeloma activity *in vitro* and *in vivo* by down-regulating the expression of class I histone deacetylases. *J. Biol. Chem.* **288**, 25593–25602 (2013).
37. Lin, Y., Devin, A., Rodriguez, Y. & Liu, Z.G. Cleavage of the death domain kinase RIP by caspase-8 prompts TNF-induced apoptosis. *Genes Dev.* **13**, 2514–2526 (1999).
38. Di, L.F., Menabo, R., Canton, M., Barile, M. & Bernardi, P. Opening of the mitochondrial permeability transition pore causes depletion of mitochondrial and cytosolic NAD<sup>+</sup> and is a causative event in the death of myocytes in postischemic reperfusion of the heart. *J. Biol. Chem.* **276**, 2571–2575 (2001).
39. Batandier, C., Leverage, X. & Fontaine, E. Opening of the mitochondrial permeability transition pore induces reactive oxygen species production at the level of the respiratory chain complex I. *J. Biol. Chem.* **279**, 17197–17204 (2004).
40. Duan, L., Gan, H., Golan, D.E. & Remold, H.G. Critical role of mitochondrial damage in determining outcome of macrophage infection with *Mycobacterium tuberculosis*. *J. Immunol.* **169**, 5181–5187 (2002).
41. Halestrap, A.P. & Davidson, A.M. Inhibition of Ca<sup>2+</sup>(+)-induced large-amplitude swelling of liver and heart mitochondria by cyclosporin is probably caused by the inhibitor binding to mitochondrial-matrix peptidyl-prolyl cis-trans isomerase and preventing it interacting with the adenine nucleotide translocase. *Biochem. J.* **268**, 153–160 (1990).
42. Osborn, S.L. *et al.* Fas-associated death domain (FADD) is a negative regulator of T-cell receptor-mediated necroptosis. *Proc. Natl Acad. Sci. USA* **107**, 13034–13039 (2010).
43. Coulombe, F. *et al.* Targeted prostaglandin E2 inhibition enhances antiviral immunity through induction of type I interferon and apoptosis in macrophages. *Immunity* **40**, 554–568 (2014).
44. Divangahi, M., Behar, S.M. & Remold, H. Dying to live: how the death modality of the infected macrophage affects immunity to tuberculosis. *Adv. Exp. Med. Biol.* **783**, 103–120 (2013).
45. Nogusa, S. *et al.* RIPK3 activates parallel pathways of MLKL-driven necroptosis and FADD-mediated apoptosis to protect against influenza A virus. *Cell Host Microbe* **20**, 13–24 (2016).
46. Tait, S.W. *et al.* Widespread mitochondrial depletion via mitophagy does not compromise necroptosis. *Cell Rep.* **5**, 878–885 (2013).
47. Newton, K. *et al.* Activity of protein kinase RIPK3 determines whether cells die by necroptosis or apoptosis. *Science* **343**, 1357–1360 (2014).
48. Stegh, A.H. *et al.* Inactivation of caspase-8 on mitochondria of Bcl-xL-expressing MCF7-Fas cells: role for the bifunctional apoptosis regulator protein. *J. Biol. Chem.* **277**, 4351–4360 (2002).
49. Gonzalez, F. *et al.* Cardiolipin provides an essential activating platform for caspase-8 on mitochondria. *J. Cell. Biol.* **183**, 681–696 (2008).
50. Schug, Z.T. & Gottlieb, E. Cardiolipin acts as a mitochondrial signalling platform to launch apoptosis. *Biochim. Biophys. Acta* **1788**, 2022–2031 (2009).
51. Niture, S.K. & Jaiswal, A.K. Inhibitor of Nrf2 (Ilnf2 or Keap1) protein degrades Bcl-xL via phosphoglycerate mutase 5 and controls cellular apoptosis. *J. Biol. Chem.* **286**, 44542–44556 (2011).
52. Nijhawan, D. *et al.* Elimination of Mcl-1 is required for the initiation of apoptosis following ultraviolet irradiation. *Genes Dev.* **17**, 1475–1486 (2003).
53. Gotow, T. *et al.* Selective localization of Bcl-2 to the inner mitochondrial and smooth endoplasmic reticulum membranes in mammalian cells. *Cell Death Differ.* **7**, 666–674 (2000).
54. Temkin, V., Huang, Q., Liu, H., Osada, H. & Pope, R.M. Inhibition of ADP/ATP exchange in receptor-interacting protein-mediated necrosis. *Mol. Cell Biol.* **26**, 2215–2225 (2006).
55. Kamata, H., Honda, S., Maeda, S., Chang, L., Hirata, H. & Karin, M. Reactive oxygen species promote TNF $\alpha$ -induced death and sustained JNK activation by inhibiting MAP kinase phosphatases. *Cell* **120**, 649–661 (2005).
56. Ricci, J.E., Waterhouse, N. & Green, D.R. Mitochondrial functions during cell death, a complex (I-V) dilemma. *Cell Death Differ.* **10**, 488–492 (2003).
57. Gleeson, L.E. *et al.* Cutting edge: *Mycobacterium tuberculosis* induces aerobic glycolysis in human alveolar macrophages that is required for control of intracellular bacillary replication. *J. Immunol.* **pii**, 1501612 (2016).
58. Machida, K., Ohta, Y. & Osada, H. Suppression of apoptosis by cyclophilin D via stabilization of hexokinase II mitochondrial binding in cancer cells. *J. Biol. Chem.* **281**, 14314–14320 (2006).
59. Woodfield, K., Ruck, A., Brdiczka, D. & Halestrap, A.P. Direct demonstration of a specific interaction between cyclophilin-D and the adenine nucleotide translocase confirms their role in the mitochondrial permeability transition. *Biochem. J.* **336** (Pt 2), 287–290 (1998).
60. Pastorino, J.G., Hoek, J.B. & Shulga, N. Activation of glycogen synthase kinase 3 $\beta$  disrupts the binding of hexokinase II to mitochondria by phosphorylating voltage-dependent anion channel and potentiates chemotherapy-induced cytotoxicity. *Cancer Res.* **65**, 10545–10554 (2005).
61. Velmurugan, K. *et al.* *Mycobacterium tuberculosis* nuoG is a virulence gene that inhibits apoptosis of infected host cells. *PLoS Pathog.* **3**, e1110 (2007).
62. Miller, J.L., Velmurugan, K., Cowan, M.J. & Briken, V. The type I NADH dehydrogenase of *Mycobacterium tuberculosis* counters phagosomal NOX2 activity to inhibit TNF- $\alpha$ -mediated host cell apoptosis. *PLoS Pathog.* **6**, e1000864 (2010).
63. Zhang, D.W. *et al.* RIP3, an energy metabolism regulator that switches TNF-induced cell death from apoptosis to necrosis. *Science* **325**, 332–336 (2009).
64. Vanlangenakker, N., Bertrand, M.J., Bogaert, P., Vandenabeele, P. & Vanden Berghe, T. TNF-induced necroptosis in L929 cells is tightly regulated by multiple TNFR1 complex I and II members. *Cell Death Dis.* **2**, e230 (2011).
65. Roca, F.J. & Ramakrishnan, L. TNF dually mediates resistance and susceptibility to mycobacteria via mitochondrial reactive oxygen species. *Cell* **153**, 521–534 (2013).
66. Barry, C.E. 3rd, *et al.* The spectrum of latent tuberculosis: rethinking the biology and intervention strategies. *Nat. Rev. Microbiol.* **7**, 845–855 (2009).
67. Divangahi, M. *et al.* NOD2-Deficient mice have impaired resistance to *Mycobacterium tuberculosis* infection through defective innate and adaptive immunity. *J. Immunol.* **181**, 7157–7165 (2008).
68. Zhu, H. *et al.* Enhancing TRAIL-induced apoptosis by Bcl-X(L) siRNA. *Cancer Biol. Ther.* **4**, 393–397 (2005).
69. Wolf, A. *et al.* Hexokinase 2 is a key mediator of aerobic glycolysis and promotes tumor growth in human glioblastoma multiforme. *J. Exp. Med.* **208**, 313–326 (2011).